

RESEARCH ARTICLE

10.1029/2018JD029529

Key Points:

- Comparisons between the derived hourly profiles from aircraft meteorological reports and nearby radiosonde data show good agreement
- The biases between two data sets are dependent on the separation distance but show little dependence on flight phases
- The aircraft measurements are accurate enough and better suited for investigating the diurnal variation of the planetary boundary layer

Correspondence to:

D. Li,
lidan@bu.edu

Citation:

Zhang, Y., Li, D., Lin, Z., Santanello, J. A., Jr., & Gao, Z. (2019). Development and evaluation of a long-term data record of planetary boundary layer profiles from aircraft meteorological reports. *Journal of Geophysical Research: Atmospheres*, 124. <https://doi.org/10.1029/2018JD029529>

Received 21 AUG 2018

Accepted 31 JAN 2019

Accepted article online 6 FEB 2019

Development and Evaluation of a Long-Term Data Record of Planetary Boundary Layer Profiles From Aircraft Meteorological Reports

Yuanjie Zhang^{1,2}, Dan Li² , Zekun Lin², Joseph A. Santanello Jr.³ , and Zhiqiu Gao¹ ¹School of Atmospheric Physics, Nanjing University of Information Science and Technology, Nanjing, China,²Department of Earth and Environment, Boston University, Boston, MA, USA, ³Hydrological Sciences Laboratory, NASA Goddard Space Flight Center, Greenbelt, MD, USA

Abstract High-quality measurements of planetary boundary layer (PBL) profiles are important for advancing our understanding of land-atmosphere coupling and PBL processes and improving the predictive capability of numerical models. Now with more than 10 years of observations from Aircraft Meteorological Data Reports (AMDAR), a decade-long (from 2007 to 2016) data record of hourly PBL profiles is developed over 54 U.S. airports. Comparisons between the derived hourly profiles and nearby radiosonde data, which are typically only available twice a day (at 00 and 12 UTC), show good agreement between the two data sets. The root-mean-square errors (RMSEs) between the AMDAR and radiosonde data are found to be dependent on the distance between the two data sets, especially at lower levels. The RMSEs of temperature generally decrease as the altitude increases, while the RMSEs of specific humidity and wind are positively correlated with the measurement magnitude. At perfect collocations (i.e., the separation distance is zero), the seasonal RMSEs at measurement levels with pressure larger than 850 hPa are 1.16–1.52 K, 0.64–1.25 g/kg, and 2.00–2.26 m/s for temperature, humidity, and wind components, respectively. Compared to the RMSEs, the mean biases of AMDAR profiles are much smaller and are less dependent on the separation distance. The RMSEs show little dependence on flight phases (ascent or descent) in the lower troposphere. Overall, our results indicate that the aircraft measurements are accurate enough to be an alternative to the radiosonde data and are better suited for investigating the diurnal variation of PBL due to their higher temporal resolution.

1. Introduction

The diurnal variations of near-surface temperature and moisture are one of the most fundamental features of Earth system and have substantial implications for agricultural and other ecosystems (Walther et al., 2002). However, capturing such a basic feature of the Earth system, especially over land, remains a grand challenge for current numerical weather and climate models (Lindvall et al., 2013; Lindvall & Svensson, 2015). This is strongly tied to model deficiencies of land-atmosphere coupling and planetary boundary layer (PBL) processes (Lindvall et al., 2013). The PBL, which is the lowest 1–3 km of the atmosphere directly influenced by the Earth's surface (Garratt, 1994; Stull, 2012), is the key link between the land and the free troposphere or the large-scale atmosphere. At diurnal scales, it serves as a short-term memory of land surface processes through the integration of surface fluxes and is a significant control on clouds and convection (Ek & Holtslag, 2004; Ek & Mahrt, 1994; Santanello et al., 2018). As a result, developing a long-term, accurate data record of PBL profiles at diurnal scales is the key to advancing our understanding of land-atmosphere coupling and PBL processes and improving the predictive capability of numerical models.

Up until now there have been no such observational data records for the PBL or more broadly the lower troposphere over land. Radiosonde measurements are usually only twice a day (mostly 00 and 12 UTC) and do not fully resolve the PBL structure. These radiosonde measurements cannot adequately characterize the diurnal cycle of the PBL, especially over the Continental United States (CONUS) where 00 and 12 UTC roughly correspond to the transitional periods between unstable and stable boundary layers. On the other hand, ground-based remote sensing from instruments such as radiometers, ceilometers, and lidar provides high temporal and vertical resolution profiling of the lower troposphere, but such measurements are often limited to a few locations and short periods. In addition, nearly all satellite data distinctly lack the temporal and vertical resolution necessary to resolve the variability within the PBL (Wulfmeyer et al., 2015).

Table 1
Summary of Uncertainties and Biases of AMDAR Data Reported by Previous Studies

	Temperature (K)	Wind speed (m/s)	Humidity (g/kg)	Error definitions	Spatial and temporal windows	Height range	Data sources
Benjamin et al. (1999)	0.49–0.77	1.6–2.5	/	Uncertainty	≤10 km, ≤10 min	900–100 hPa	AMDAR data near Denver airport terminal area from August 1996 to August 1997
Drüe et al. (2008)	0.25–0.72	0.6–2	/	Uncertainty	≤1 hr	1–4 km	AMDAR descent data at Frankfurt airport on 22 days in 2004
Ballish and Kumar (2008)	1.00–1.47	/	/	Uncertainty	/	1,000–150 hPa	AMDAR data used by the NCEP Global Data Assimilation System at 00 and 12 UTC from July 2002 to June 2005
Petersen et al. (2016)	/	/	~0.2	Uncertainty	≤15 km, ≤15 min	1,000–300 hPa	WVSS data at the Rockford airport, Illinois, during 16 evenings over three separated periods in fall 2009, spring 2010, and summer 2010
Schwartz and Benjamin (1995)	0.97	5.76	/	RMSE from radiosonde data	≤150 km, ≤90 min	1,829–9,144 m	AMDAR and radiosonde data collected around Denver airport in February and March 1992
Ballish and Kumar (2008)	~0.5–1			MBE from radiosonde data	≤200 km, ≤90 min	250 ± 25 hPa	AMDAR and radiosonde data over CONUS at 00 and 12 UTC January 2007
Drüe et al. (2010)	<0.5	~2.5	/	MBE from radar data	≤60 min	≤1,800 m	AMDAR and WTR/RASS measurements at Frankfurt airport in 2006
Ding et al. (2015)	1.40	3.56	/	RMSE from radiosonde data	≤100 km, ≤15 min	≥200 hPa	AMDAR data over China and radiosonde data from 10 stations from 1 January 2004 to 31 December 2010
Petersen et al. (2016)	/	/	0.62	RMSE from radiosonde data	≤50 km, ≤60 min	1,000–300 hPa	WVSS and radiosonde data at the Rockford airport, Illinois, during 16 evenings over three separated periods in fall 2009, spring 2010, and summer 2010

Note. “/” indicates null.

The other data source that provides routine observations of PBL profiles is the Aircraft Meteorological Data Reports (AMDAR), which is the term used for automated weather reports from commercial aircraft globally (Moninger et al., 2003). The data link system between aircraft and airline is known as the Aircraft Communications Addressing and Reporting System (ACARS), and hence, the AMDAR data are also often referred to as the ACARS data, especially in the U.S. For consistency, we use the term AMDAR throughout the paper. Nowadays there are more than 600,000 temperature and wind observation points (not profiles) available per day, 450,000 of which are over CONUS. Compared to temperature and wind observations, the humidity observations are much less in number but still cover many parts of CONUS thanks to the newly developed Water Vapor Sensing System (WVSS; Petersen et al., 2016).

Unlike radiosonde data that are typically only available twice a day (at 00 and 12 UTC), the AMDAR program provides vertical profiles (through ascents and descents made at airports) at considerably higher temporal resolutions, which can be used to characterize the diurnal variation of the PBL (Rahn & Mitchell, 2016). So far, the most important application of AMDAR data has been assimilation into numerical weather prediction models for improving short-term forecasts (Cardinali et al., 2003; Moninger et al., 2003; Petersen, 2016; Petersen et al., 2016; Zhu et al., 2015). However, their use as an observational data record for land-atmosphere coupling and PBL research is very sparse. Now with more than 10 years of AMDAR data, constructing a long-term data record of PBL profiles that resolve the diurnal cycle becomes feasible with this data set, which frames the scope of this study.

Unlike the quality of radiosonde data that has been subject to a large number of studies (Corner et al., 1999; Ingleby et al., 2016; Mapes et al., 2003; Miloshevich et al., 2001), only a small number of studies have investigated the quality of AMDAR data (e.g., Benjamin et al., 1999; Drüe et al., 2008). They assessed the accuracy of AMDAR data by comparing them against radiosonde data (Ding et al., 2015; Schwartz & Benjamin, 1995), wind profiler radar data (Drüe et al., 2010), or model-simulated fields (Ballish & Kumar, 2008; Moninger et al., 2010, 2003). A summary of findings from previous studies is presented in Table 1, in which and

throughout this paper *uncertainty* describes the variability of AMDAR data (e.g., among aircraft types and ascents/descents), while *bias* is defined as the root-mean-square error (RMSE) or the mean bias error (MBE) between the AMDAR data and the reference data (e.g., radiosondes).

A comparison between AMDAR and radiosonde data collected around the Denver airport by Schwartz and Benjamin (1995) revealed that temperatures and winds in AMDAR ascent/descent profiles agree well with radiosonde soundings. The RMSEs of temperature and wind decrease from 0.97 K and 4.08 m/s to 0.59 K and 2.84 m/s, respectively, as the distance (time) separation between AMDAR and radiosonde data shortens from 150 km (90 min) to 25 km (15 min). Also, at the Denver airport, Benjamin et al. (1999) performed a collocation study by examining the differences between pairs of AMDAR reports from different aircrafts with small spatial (≤ 10 km) and temporal (≤ 10 min) separation and found that the uncertainties, determined as the RMSEs between pairs of AMDAR data, are 0.49–0.77 K for temperature and 1.6–2.5 m/s for wind speed. Ding et al. (2015) compared temperature and wind observations between AMDAR reports and radiosonde data over east China and found that the RMSEs are 1.40 K for temperature, 3.56 m/s for wind speed, and 28 degrees for wind direction.

In addition, Drüe et al. (2008) found that the AMDAR data are dependent upon the aircraft type and the temperature measurements made by different aircraft types can differ by up to 1 K. Studies also show that ascent temperatures are warmer than descent temperatures in AMDAR reports (Ballish & Kumar, 2008; Schwartz & Benjamin, 1995) and wind differences between AMDAR and radiosonde data are smaller for descents than for ascents (Ding et al., 2015; Schwartz & Benjamin, 1995). A recent review study (Petersen et al., 2016) suggested that the AMDAR humidity data observed by WVSS are at least as accurate as radiosonde observations. The WVSS observations agree with collocated radiosonde data within 0.6 g/kg and show consistency between different aircrafts of about 0.2 g/kg when the distance and time separation are less than 15 km and 15 min, respectively.

These previous studies suggest that the AMDAR data generally have a high degree of accuracy and the differences between AMDAR data and radiosonde data vary with aircraft types, pressure levels, phase of flights, and the distance and time separation. However, these comparisons are often limited to short periods or a small number of locations (see Table 1). This study aims to generate a decade-long (from 2007 to 2016) data record of hourly PBL temperature, humidity, and wind profiles near major U.S. airports based on the AMDAR data and thoroughly validate the new data product through comparisons to radiosonde data. The comparison between AMDAR and radiosonde data is conducted for different locations, seasons, and pressure levels. The new data product fills in a much needed gap in our observational suite and supports both research and operational applications in terms of understanding and predicting land-atmosphere coupling and PBL processes.

2. Data and Methods

2.1. Raw Data

The AMDAR program was established by the World Meteorological Organization (WMO) in cooperation with aviation partners and has led to the development of the AMDAR observing system. Automated meteorological reports first became available in 1979 and have increased dramatically in the 1990s (Moninger et al., 2003). The AMDAR system now produces observations from over 40 participating airlines, which include high-resolution vertical profiles of air temperature and wind speed and direction at airports, regular reports of meteorological variables from airplanes at cruise level, accurate measurements of coordinates (time, latitude, longitude, and pressure altitude), and an increasing number of humidity and turbulence measurements. Currently, the AMDAR temperature and wind data come from approximately 5,000 aircraft per day (Petersen, 2016), while 148 aircraft-based WVSS deliver humidity observations operationally across the globe daily, principally over CONUS (Petersen et al., 2016).

The archived AMDAR data, which are older than 48 hr, are publicly available through the Meteorological Assimilation Data Ingest System (MADIS), which can be accessed through the MADIS web service portal (<https://madis-data.cprk.ncep.noaa.gov/madisPublic1/data/archive/>). These data are stored hourly (i.e., 24 individual files per day), and each hour/file includes a certain number of sounding profiles. The aircraft data set is organized in two different ways: the *Aircraft-Based Reports* files contain all the raw data as individual

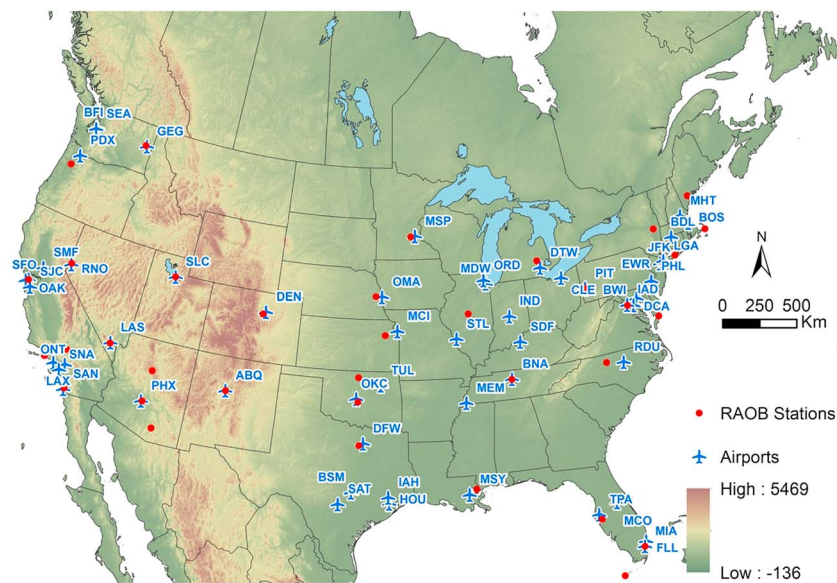


Figure 1. The distribution of selected airports with AMDAR data (blue symbols) and the matched radiosonde stations (red dots) over the CONUS.

point measurements, while the *Profiles at Airports* files contain only data taken from aircraft ascents and descents near airports, which are organized into profiles/soundings associated with the location of the airports. In this study, the latter is used given our focus on the PBL structures.

The AMDAR data are temporally and spatially variable. Evening peaks and early morning minima of commercial air traffic cause the total number of reports per hour to vary by over a factor of 4 (Moninger et al., 2003). Some airports have relatively fewer reports due to its smaller traffic flow and lack of measurement in early morning hours. Therefore, we conduct a selection for airports and require airports to have reports in at least 20% of the total hours in each year during 2007–2016 over CONUS. Based on this criterion, 54 airports are selected as shown in Figure 1. These selected airports cover a range of climatic zones but are mainly located in the northeast, along the west coast, and in the central U.S.

The radiosonde data operated by the Universal RAwinsonde OBservation (RAOB) program, which are also available publicly on the MADIS web service portal, enable comparisons between AMDAR and radiosonde measurements. Although the radiosonde data are archived hourly, the observations are usually only available at 00 and 12 UTC. In this study, the radiosonde data at the 22 mandatory levels are used, which include 10 pressure (p) levels larger or equal to 200 hPa (surface, 1,000, 925, 850, 700, 500, 400, 300, 250, and 200 hPa). In addition to the mandatory levels, radiosonde data at significant levels are also available in the MADIS archive. The significant levels are where the vertical profiles of temperature or humidity vary appreciably from a straight line. The significant levels for $p > 200$ hPa vary from profile to profile, but their number is on the order of 10–20 per profile. We conducted comparisons between the AMDAR and radiosonde data when the radiosonde data at both mandatory and significant levels are used. Including the significant levels did not change our findings. As such, we decided to only use data at mandatory levels for the presented statistical analysis, which avoids interpolation when the radiosonde data from different times are averaged (see, e.g., Figure 4).

The RAOB stations have to be within 200 km from the airports for comparison purposes following Ballish and Kumar (2008). If there are more than one RAOB stations that are less than 200 km from the selected airport, each RAOB station is paired with the airport. Finally, 37 RAOB stations, shown as red dots in Figure 1, are selected to pair with 43 airports. Note that one RAOB station could be matched to several airports simultaneously in areas where airports are close to each other. Also note that the distance between the airport and the collocated radiosonde station is calculated by the square root of their longitude and latitude difference, and 1° difference in longitude/latitude is considered to be approximately 100 km. The geographic information of the selected airports and RAOB stations and their separation distances are given in Table 2.

Table 2
Geographic Information of the Selected Airports and the Collocated Radiosonde Stations and Their Separation Distances

	IATA code	Airport name	AMDAR_lat (°N)	AMDAR_long (°E)	RAOB_lat (°N)	RAOB_long (°E)	Distance (km)
1	ABQ	Albuquerque International Sunport	35.05	-106.62	35.05	-106.6	2
2	BDL	Bradley International Airport	41.93	-72.68	40.87	-72.87	108
					42.75	-73.8	139
3	BFI	Boeing Field	47.53	-122.30	/	/	/
4	BNA	Nashville International Airport	36.13	-86.68	36.12	-86.68	1
5	BOS	Boston Logan International Airport	42.36	-71.01	41.67	-69.97	125
					43.88	-70.25	170
6	BSM	Austin-Bergstrom International Airport	30.20	-97.68	/	/	/
7	BWI	Baltimore/Washington International Thurgood Marshall Airport	39.18	-76.67	39.47	-76.17	58
					38.95	-77.45	81
					37.85	-75.48	178
8	CLE	Cleveland Hopkins International Airport	41.41	-81.86	40.5	-80.22	188
9	DCA	Ronald Reagan Washington National Airport	38.85	-77.03	38.95	-77.45	43
					39.47	-76.17	106
					37.85	-75.48	184
10	DEN	Denver International Airport	39.87	-104.67	39.75	-104.87	23
11	DFW	Dallas/Fort Worth International Airport	32.90	-97.03	32.8	-97.3	29
12	DTW	Detroit Metropolitan Wayne County Airport	42.23	-83.33	42.68	-83.47	47
13	EWB	Newark Liberty International Airport	40.70	-74.17	40.87	-72.87	131
14	FLL	Fort Lauderdale-Hollywood International Airport	26.07	-80.15	25.82	-80.28	28
15	GEG	Spokane International Airport	47.63	-117.53	47.68	-117.63	11
16	HOU	William P. Hobby Airport	29.65	-95.28	/	/	/
17	IAD	Dulles International Airport	38.98	-77.47	38.95	-77.45	4
					39.47	-76.17	139
18	IAH	George Bush Intercontinental Airport	29.97	-95.35	/	/	/
19	IND	Indianapolis International Airport	39.73	-86.27	/	/	/
20	JFK	John F. Kennedy International Airport	40.65	-73.78	40.87	-72.87	94
21	LAS	McCarran International Airport	36.08	-115.17	36.05	-115.18	3
22	LAX	Los Angeles International Airport	33.93	-118.40	34.12	-119.12	74
					34.9	-117.88	110
23	LGA	LaGuardia Airport	40.77	-73.87	40.87	-72.87	100
					42.75	-73.8	198
24	MCI	Kansas City International Airport	39.32	-94.72	39.07	-95.62	93
25	MCO	Orlando International Airport	28.43	-81.32	28.47	-80.55	77
					27.7	-82.4	130
26	MDW	Chicago Midway International Airport	41.78	-87.75	/	/	/
27	MEM	Memphis International Airport	35.05	-90.00	/	/	/
28	MHT	Manchester-Boston Regional Airport	42.93	-71.43	43.88	-70.25	151
					41.67	-69.97	193
29	MIA	Miami International Airport	25.82	-80.28	25.82	-80.28	0
					24.55	-81.75	194
30	MSP	Minneapolis–Saint Paul International Airport	44.88	-93.22	44.85	-93.57	35
31	MSY	Louis Armstrong New Orleans International Airport	29.98	-90.25	30.25	-89.77	55
32	OAK	Oakland International Airport	37.73	-122.22	37.73	-122.22	0
33	OKC	Will Rogers World Airport	35.40	-97.60	35.23	-97.47	21
					36.62	-97.48	123
34	OMA	Eppley Airfield	41.30	-95.90	41.32	-96.37	47
35	ONT	Ontario International Airport	34.05	-117.62	34.9	-117.88	89
					32.82	-117.13	132
36	ORD	O'Hare International Airport	41.98	-87.90	/	/	/
37	PDX	Portland International Airport	45.60	-122.60	44.92	-123	79
38	PHL	Philadelphia International Airport	39.87	-75.24	39.47	-76.17	101
39	PHX	Phoenix Sky Harbor International Airport	33.43	-112.02	33.45	-111.95	7
					32.12	-110.93	170
					35.23	-111.82	181

Table 2 (continued)

IATA code	Airport name	AMDAR_lat (°N)	AMDAR_long (°E)	RAOB_lat (°N)	RAOB_long (°E)	Distance (km)
40	PIT Pittsburgh International Airport	40.50	−80.23	40.5	−80.22	1
41	RDU Raleigh-Durham International Airport	35.87	−78.78	36.08	−79.95	119
42	RNO Reno-Tahoe International Airport	39.50	−119.78	39.57	−119.78	7
43	SAN San Diego International Airport	32.73	−117.17	32.82	−117.13	10
44	SAT San Antonio International Airport	29.53	−98.47	/	/	/
45	SDF Louisville International Airport	38.18	−85.73	/	/	/
46	SEA Seattle-Tacoma International Airport	47.45	−122.30	/	/	/
47	SFO San Francisco International Airport	37.62	−122.38	37.73	−122.22	19
48	SJC Norman Y. Mineta San Jose International Airport	37.37	−121.92	37.73	−122.22	47
49	SLC Salt Lake City International Airport	40.77	−111.97	40.78	−111.97	1
50	SMF Sacramento International Airport	38.70	−121.60	37.73	−122.22	115
51	SNA John Wayne Airport	33.67	−117.88	32.82	−117.13	113
				34.9	−117.88	123
52	STL St. Louis Lambert International Airport	38.74	−90.36	40.15	−89.33	175
53	TPA Tampa International Airport	27.97	−82.53	27.7	−82.4	30
54	TUL Tulsa International Airport	36.20	−95.90	36.62	−97.48	163
				35.23	−97.47	185

Note. “/” indicates that no radiosonde station is found to match the airport.

2.2. From Raw Data to a Single Profile at Regular Pressure or Height Levels

There are large variations in terms of the number of soundings among airports. For temperature and wind measurements, the annual number of soundings has experienced a pronounced increase since 2007 over most airports, and nine airports (BWI, DEN, DFW, HOU, LAS, LAX, MDW, PHX, and SEA) have more than 100,000 soundings in 2016. But at some airports, such as CLE, DTW, IAD, and MSP (see Table 2 for their full names), the annual number of soundings decreased from 2007 to 2016. The number of soundings with humidity measurements is much less. Although it has increased over most airports, but at several airports, such as DTW, MSP, and SEA, the sounding number was larger before 2011 and then decreased. It should be noted that there are hardly any humidity measurements available in 2015 and 2016 from the AMDAR data set.

The raw AMDAR data are quite irregular. On one hand, the sampling rate varies from 10 s to 30 min (Benjamin et al., 1999; Drüe et al., 2008). On the other hand, for some soundings there may be very few data points located at very sparse levels or within a small height range. This might be because spurious measurements (e.g., those collected when the pitot tubes are corroded or clogged with debris) may have been removed in the preprocessing by MADIS (Ballish & Kumar, 2008). This issue is more prominent for humidity due to the much less data points to begin with. Some studies chose to remove soundings that do not meet their criteria (Rahn & Mitchell, 2016), which may remove some reasonable data points and thus reduce the sample size.

In this study, we choose to merge all the soundings within an hour into one profile by assuming that the variations of AMDAR measurements within an hour are small. We do not separate different aircraft types and flight phases for two reasons. First, most of the radiosonde data are limited to 00 and 12 UTC and thus some aircraft types may not even have data in those two hours. Second, separating different aircraft types or flight phases would reduce the robustness of interpolation because the number of data points would be significantly reduced. Our choice is also supported by a previous study finding that the random errors of AMDAR temperature measurements are less than 0.3 K by comparing single soundings to hourly averaged profiles (Drüe et al., 2008). However, we do remove data points that are more than 15 km away from the airport and are also below 1500 m, as there may be large horizontal variations in the PBL due to changes in local surface conditions such as topography and land cover. After the merge, we further require the profile to have at least 10 measurements under 1,500 m and at least one measurement within 200 m from the surface following Rahn and Mitchell (2016). The annual averaged number of valid hourly profiles after the merge is shown

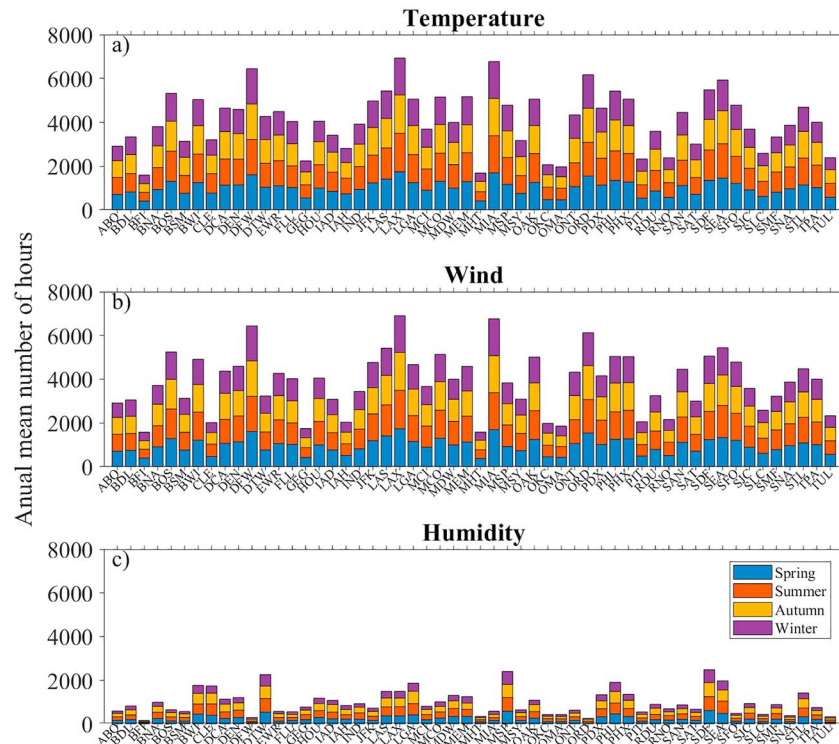


Figure 2. Annual mean numbers of hourly profiles of temperature (top panel), wind (middle panel), and humidity (bottom panel) at the selected airports during the period 2007–2016.

in Figure 2. As can be seen, there are no significant seasonal differences in terms of the annual averaged number of hourly profiles. Note that in this study spring, summer, fall, and winter are defined as December–February, March–May, June–August, and September–November, respectively.

Since the vertical sampling interval by each aircraft is variable, all measurement points are interpolated onto regular pressure (or height) levels that increase from the surface by 20 hPa (or 20-m) intervals. The 20 hPa (or 20 m) is a relatively fine resolution, which is used to capture the observations near the surface (Rahn & Mitchell, 2016). Figure 3 shows two examples (one during convective conditions and the other during stable conditions) of the interpolated profiles (on regular height levels) and the raw soundings. It can be seen that, in general, there are more measurements in lower levels, which is in favor of PBL investigations. The black symbols indicate the removed data points due to their large horizontal distance from the airport (recall that we remove data points when they are more than 15 km away from the airport and are also below 1500 m). But it can be seen that at this location there is no significant difference between the removed data points and the interpolated profile, as most of the removed data points are still within the standard deviation represented by the shading.

An example of the diurnal and day-to-day evolution of AMDAR potential temperature in June 2016 at EWR from the surface to 3,000 m above the surface is shown in Figure 3c. The blank areas are hours when there is no data, which often occur around midnight but do not occupy a significant portion. In this figure, the diurnal cycle of potential temperature is evident within the PBL especially on clear days (e.g., on 15 and 29 June). One can also see the rich PBL structures such as the cold and hot plumes, as well as the strongly variable interface between the PBL and the free atmosphere, at both diurnal and day-to-day time scales. Such features are extremely difficult, if not impossible, to identify with the available radiosonde data. This example highlights that compared to the radiosonde data, the generated data record based on AMDAR data has a unique advantage in resolving the diurnal variation and the vertical structure of the PBL.

It should be noted that the vertical position of aircraft in the AMDAR data is given as the pressure altitude, which is determined from the measured static pressure using a standard atmosphere. The pressure altitude may depart greatly from the true height and may even appear below the sea level. It is reasonable that

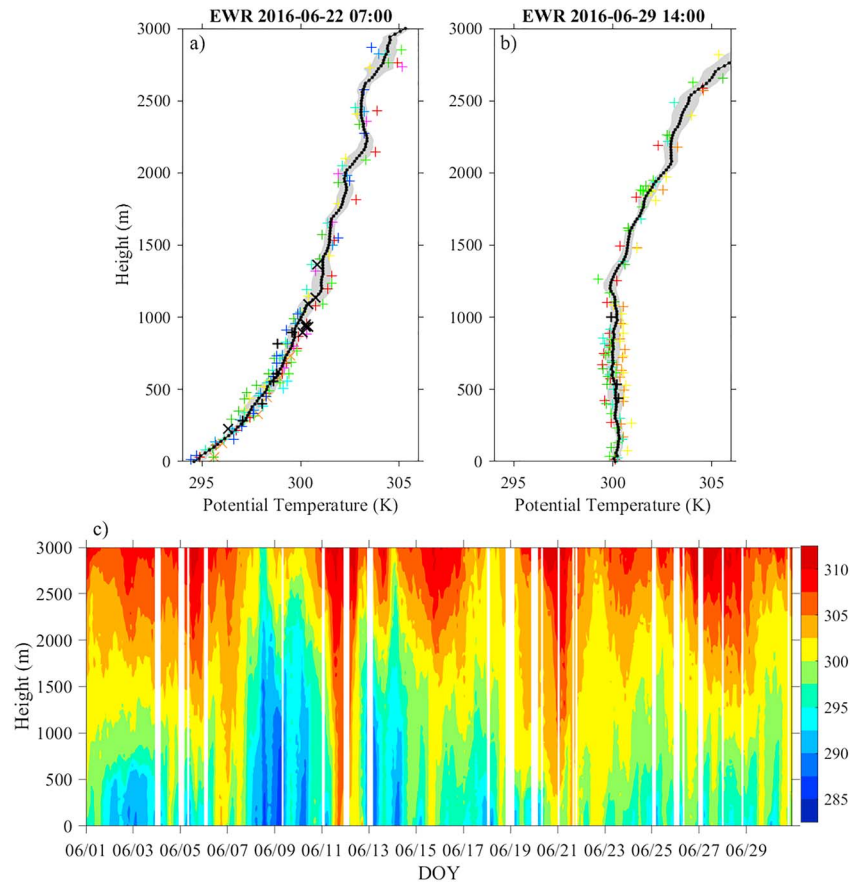


Figure 3. The interpolated hourly potential temperature profiles and raw soundings at EWR at (a) 0700 LST 22 June 2016 (stable PBL) and (b) 1400 LST 29 June 2016 (unstable PBL). (c) The potential temperature in the lowest 3,000 m above the ground at EWR from 1 to 30 June 2016. In (a) and (b), black bold dash-dotted line indicates the interpolated hourly profile. Ascent and descent soundings are indicated by plus signs and multiplication signs, respectively, and different symbol colors represent different soundings, with the black symbols indicating the removed data points due to their large distances from the airport. The shade shows the standard deviation of the interpolated profile. The blank areas in (c) indicate hours that have no data.

sometimes the pressure altitude is negative when the actual pressure near the surface is greater than the standard atmospheric pressure. Thus, before the previously described height interpolation, the pressure altitude should be converted to the height. To do so, the pressure altitude (z_p) is first converted to pressure (p) via the following equation (WMO, 2003):

$$p = 1013.25 \left(1 - \frac{z_p \cdot K_f}{145366.45} \right)^{5.2553}, \quad (1)$$

with the feet-to-meter conversion factor $K_f = 0.3048$. Then the actual height is calculated by integrating the hypsometric equation from the surface upward using the pressure calculated by equation (1), the temperature measurements from the aircraft, and the surface temperature and pressure from the Integrated Surface Database (ISD) provided by National Oceanic and Atmospheric Administration (NOAA) at <https://www.ncdc.noaa.gov/isd/data-access>. This data set has a high degree of accuracy and reliability as strict quality control has been imposed on the input data sources and the entire ISD archive (Lott, 2004). There are a few but very rare instances where the computed height is still negative as the pressure measured by the aircraft is higher than the pressure measured the surface meteorological station. This is possibly due to the instrumental error or some other measurement uncertainty. However, the negative values rarely occur and are small (the absolute values are mostly less than 10) and hence will not lead to significant errors in the interpolated profiles.

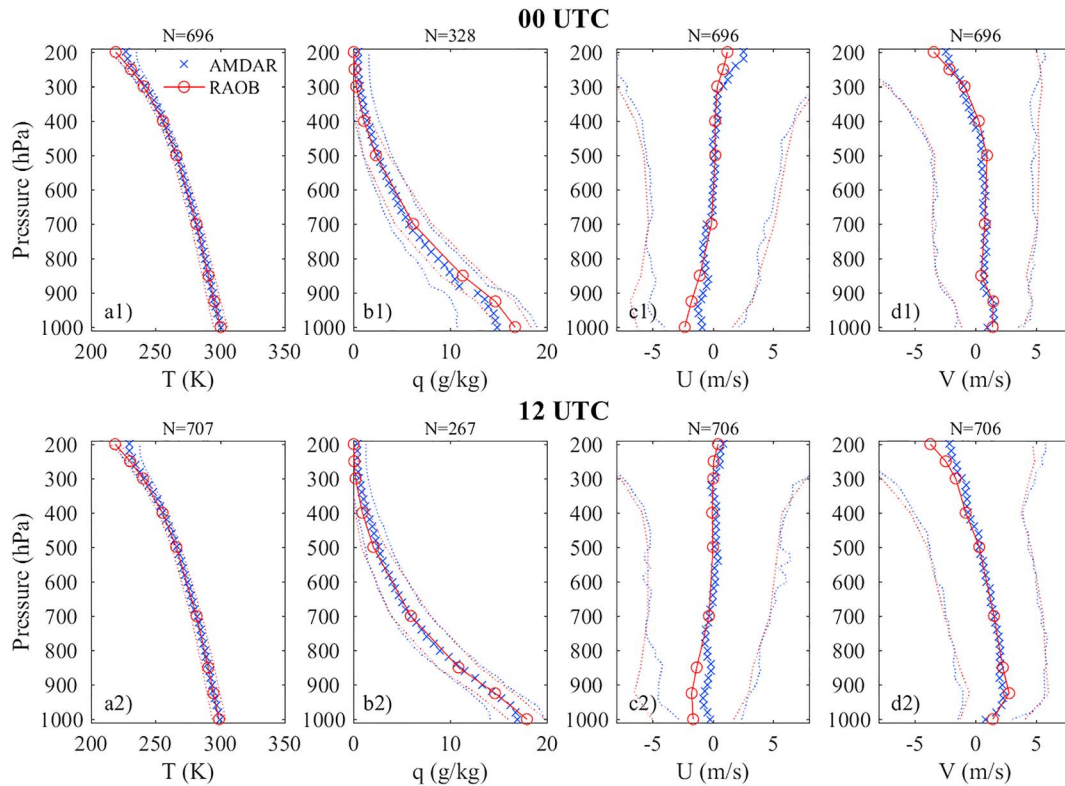


Figure 4. Ten-year (from 2007 to 2016) averaged AMDAR and radiosonde profiles at 00 (top) and 12 UTC (bottom) in summer over Miami (MIA) international airport. (a) Temperature (T), (b) specific humidity (q), (c) zonal wind (U), and (d) meridional wind (V). N indicates the number of profiles. Red and blue dot lines indicate the standard variations of AMDAR and radiosonde profiles, respectively.

3. Results

Since AMDAR and radiosonde data do not have the same temporal and vertical resolutions, comparisons can only be conducted for the hours when both data sources are available (mostly 00 and 12 UTC). As an example, Figure 4 shows the 10-year (from 2007 to 2016) averaged AMDAR and radiosonde profiles at 00 and 12 UTC in summer at the Miami (MIA) international airport. It is clear that overall, the AMDAR data agree reasonably well with the radiosonde data in terms of mean and variability. Detailed statistical analysis of the comparison between AMDAR and radiosonde data will be presented later. Note that here the radiosonde data at the surface pressure level are not used because the surface pressure level changes from hours to hours.

To investigate the dependence of AMDAR biases on climatic conditions and pressure levels, the comparison is conducted separately for different seasons and pressure ranges. Specifically, four different pressure ranges are chosen (i.e., larger than 850, 850–500, 500–300, and 300–200 hPa). Data from levels with $p < 200$ hPa are not included because they are sparse in both AMDAR and radiosonde data sets. As mentioned above, separation in distance between AMDAR and radiosonde data is limited to be less than 200 km. Although this limit is larger than those in some previous studies (Ding et al., 2015; Schwartz & Benjamin, 1995), it is pointed out that only 12 of 61 pairs have separation distances larger than 150 km and 23 of them are less than 50 km (Table 2). The comparison results will be presented in terms of linear regression coefficient, goodness of fit (or R^2), MBE (AMDAR minus radiosonde), and RMSE.

We discuss the results on temperature, humidity, and wind separately. The results from a few airports that have large numbers of data points (Figure 2) and small distances between airports and radiosonde stations (Table 2) are first presented as case studies, and then the discussion is extended to the entire data set. In each subsection, the dependence of the AMDAR-radiosonde comparison on the separation distance, pressure range, and season are examined. Sections 3.4 and 3.5 are devoted to examining the differences between

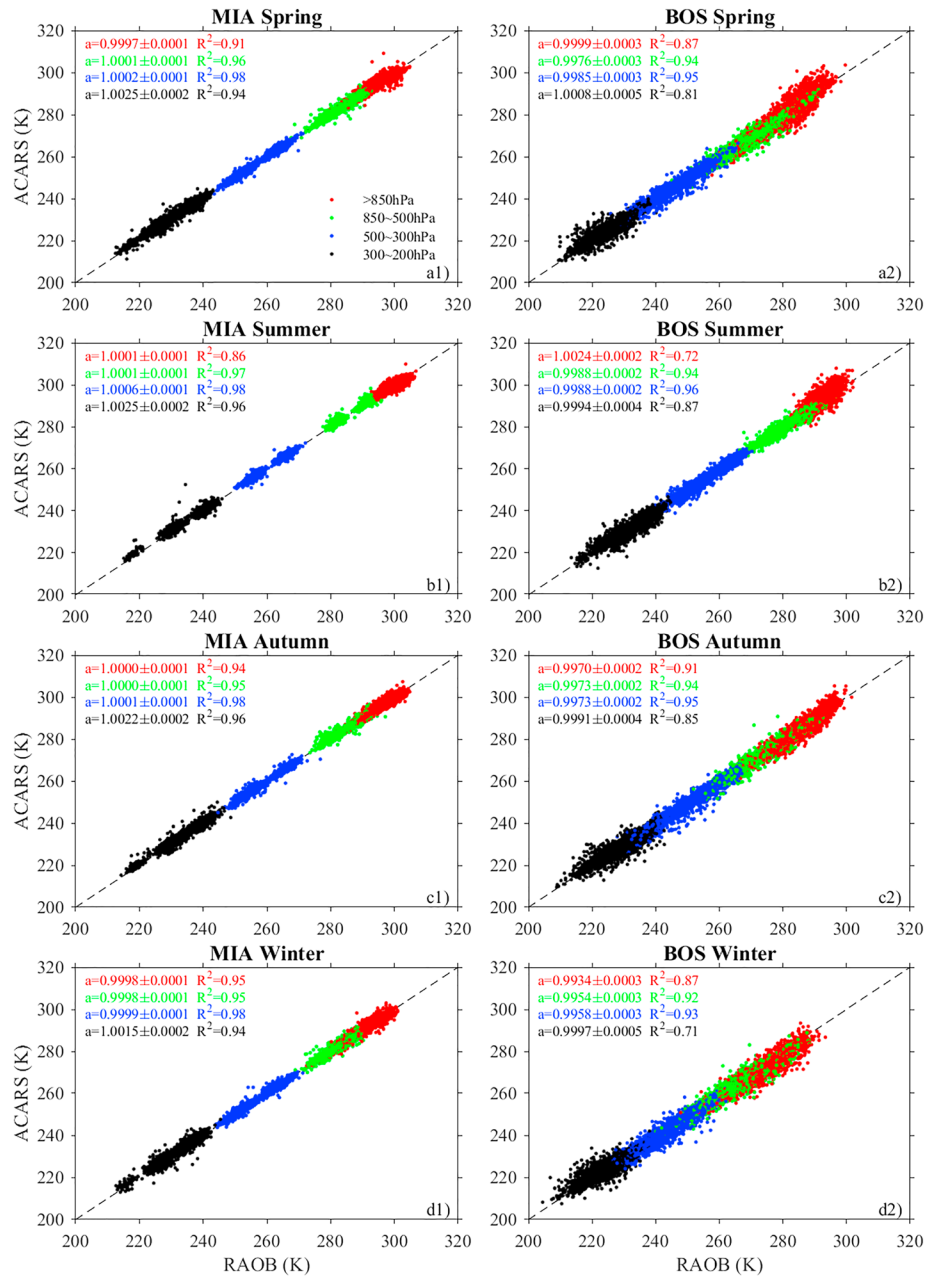


Figure 5. Comparisons between AMDAR and RAOB temperature data in different pressure ranges and seasons (from top to bottom: spring, summer, autumn, and winter) at MIA (left) and BOS (right).

ascents and descents and demonstrating the unique value of the new data record of PBL profiles in studying the diurnal variation of the PBL, respectively.

3.1. Temperature

Figure 5 presents one-to-one comparisons between AMDAR and radiosonde data during the study period from 2007 to 2016 at Miami (MIA) and Boston (BOS) international airports. It is clear that there is a close agreement between the two data sets. Here simple linear regression without an intercept ($y = ax$) is conducted for each season and pressure range, so that the value of the slope a indicates overestimation (underestimation) of AMDAR observations when a is larger (smaller) than 1, with the caveat that its value is dependent on the temperature magnitude itself. It can be seen at both MIA and BOS, a is very close to 1.

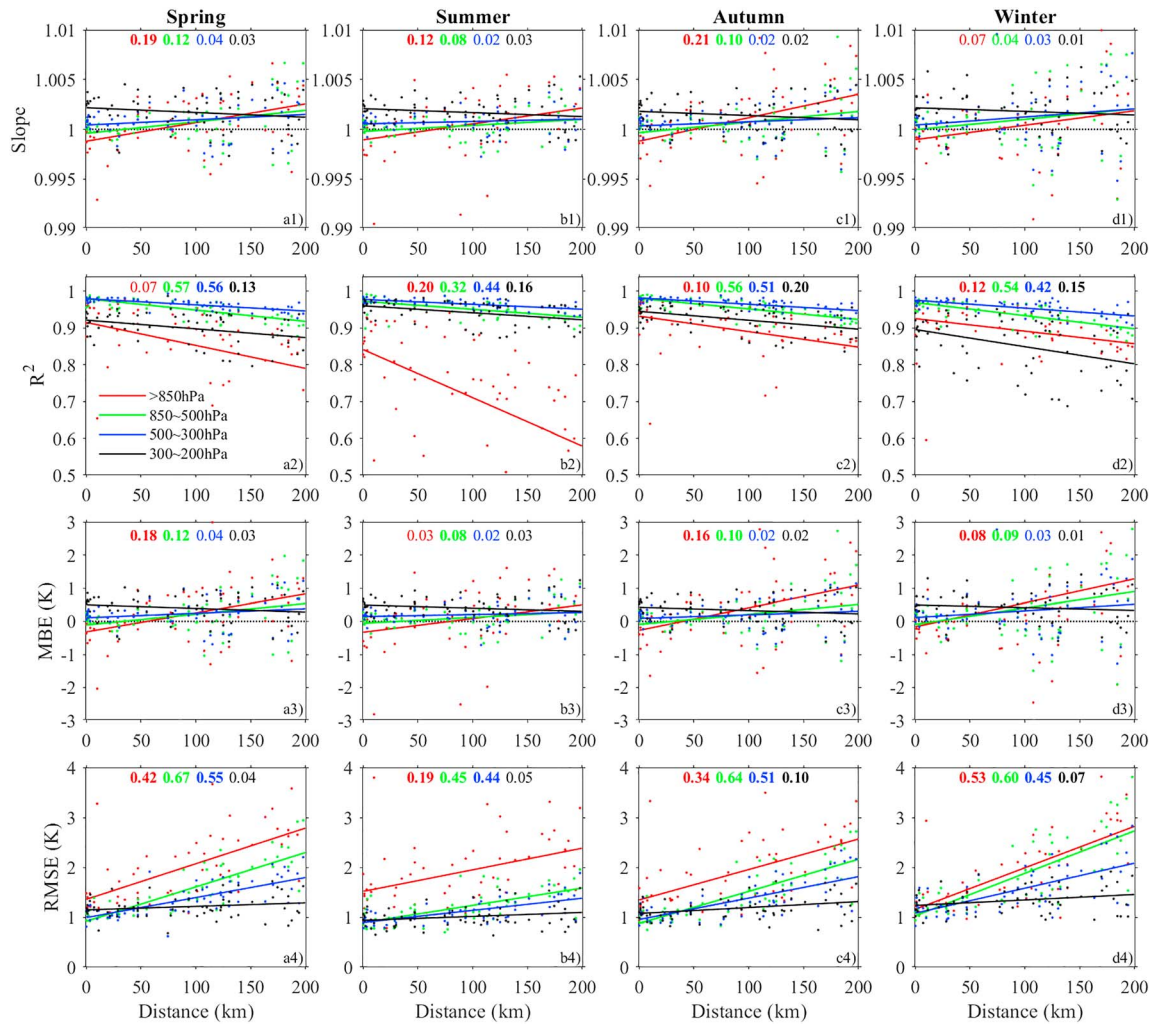


Figure 6. Relations between the fitting slopes (a1–d1), the goodness of fit (a2–d2), MBEs (a3–d3), and RMSEs (a4–d4) at four different pressure ranges and the distance between AMDAR airports and RAOB stations in (a) spring, (b) summer, (c) autumn, and (d) winter. The results are for air temperature. The numbers in each panel indicate the goodness of fit for the linear relationships for the pressure ranges with $p > 850$, 850–500, 500–300, and 300–200 hPa, respectively. The numbers in bold represents the linear trends are significant.

The R^2 values are all above 0.9 and are larger in the middle pressure ranges (500–300 and 850–500 hPa) at both airports. The fit is a little bit worse in the lowest pressure range ($p > 850$ hPa). The lower R^2 values in the pressure range with $p > 850$ hPa are expected given the stronger variability associated with the PBL than the free atmosphere. Compared to the results at MIA, the results at BOS are slightly worse. This is because the radiosonde station near MIA is located just at the airport, while the radiosonde station near BOS is 125 km far away. In particular, the warmer biases in the pressure range with $p > 850$ hPa at BOS in summer may reflect the influence of urban heat island on the PBL (Oke, 1982), which is only sensed by the AMDAR data but not the radiosonde data. It should be noted here that the BOS airport and the reference RAOB station are both located close to the land-sea boundary (the RAOB station is located on Cape Cod) and hence are potentially influenced by the ocean in a similar way. This may be why the comparison results at BOS are quite good, despite the relatively large separation distance. This is different from the results at some other coastal airports such as the SAN airport, which has an inland reference RAOB station. The results at the SAN airport will be discussed later.

To summarize the results over all the airports, Figure 6 shows the fitting statistics as a function of the distance between AMDAR and radiosonde stations for each pressure range and each season. The numbers in each panel indicate the goodness of fit for the linear relationships, whose color represents the

Table 3

The RMSEs and MBEs for Temperature, Specific Humidity, U , and V in Each Season When the Separation Distance and the Pressure Range Are 0 km and With $p > 850$ hPa or <10 km and with $p > 500$ hPa

Season	Separation distance (km)	Pressure altitude (hPa)	Temperature		Humidity		U		V	
			MBE (K)	RMSE (K)	MBE (g/kg)	RMSE (g/kg)	MBE (m/s)	RMSE (m/s)	MBE (m/s)	RMSE (m/s)
Spring	0	>850	-0.31	1.35	0.01	0.85	-0.55	2.25	-0.17	2.26
	<10	>500	-0.11	1.20	-0.01	0.76	-0.56	2.53	0.04	2.54
Summer	0	>850	-0.32	1.52	0.01	1.25	-0.68	2.26	-0.29	2.18
	<10	>500	-0.10	1.22	0.05	1.25	-0.49	2.33	-0.03	2.33
Autumn	0	>850	-0.27	1.34	-0.01	0.98	-0.48	2.11	-0.01	2.00
	<10	>500	-0.09	1.17	-0.01	0.97	-0.46	2.27	0.02	2.30
Winter	0	>850	-0.16	1.16	0.02	0.64	-0.54	2.11	0.13	2.15
	<10	>500	0.04	1.18	0.01	0.57	-0.49	2.40	0.14	2.38

corresponding pressure range. The numbers in bold imply that the linear trends pass the Mann-Kendall test at a 0.05 significance level. First, it is clear that the fitting slopes in the lowest pressure range ($p > 850$ hPa) show an increasing trend with the distance from slightly below 1 to above 1. This means that compared to the radiosonde data, the AMDAR data gradually show warmer bias as the distance becomes larger. Such an increasing trend is again consistent with the expectation that the urban influence on the PBL is only sensed by the AMDAR data but not the radiosonde data (Oke, 1982), as the reference radiosonde data are often collected in a more rural location when the separation distance is large. As a result, when the separation distance becomes large, the AMDAR data appear warmer. On the other hand, the fitting slopes for three higher pressure ranges (850–500, 500–300, and 300–200 hPa) have no significant trends with distance (Figures 6a1–6d1). This is because the free atmosphere is less affected by local surface conditions and is more uniform. Similar results are indicated by the MBEs between AMDAR and radiosonde (AMDAR-radiosonde) shown in Figures 6a3–6d3.

The slopes for $p < 500$ hPa are all larger than unity, indicating warm biases in the AMDAR data. This is consistent with previous studies arguing that the AMDAR temperature data have warm biases (Ballish & Kumar, 2008), which are recognized by a recent review paper (Petersen, 2016) and several numerical weather prediction centers (e.g., Isaksen et al., 2012; Zhu et al., 2015). However, after thoroughly comparing our results to previous studies, including a recent study examining the temperature profiles at three Southern California airports (Rahn & Mitchell, 2016), we find that such warm biases seem to occur mostly at high altitudes (i.e., at low-pressure levels). For example, the widely cited study by Ballish and Kumar (2008) focused on the tropopause region (250 ± 25 hPa) and only used data from two months (January and July 2007). The reason that their study focused on the tropopause region is probably because the AMDAR data are abundant during the cruise phase (i.e., near the tropopause). In our study (and also the study by Rahn and Mitchell, 2016), we consider data near the airport (i.e., during the ascent and descent phases, not the cruise phase) and do not focus on any particular pressure level. As a result, our finding that warm biases occur at high altitudes but are insignificant at low altitudes is consistent with previous studies and makes AMDAR data even better suited for studying PBL processes.

The goodness of fit is acceptable for most airports at all pressure levels and shows decreasing trends with increasing separation distance as expected (Figures 6a2–6d2). The drop of R^2 with increasing separation distance is particularly significant in the lowest-pressure range ($p > 850$ hPa) in summer. The RMSEs are mostly less than 3 K and show significantly increasing trends with distance in the lower three pressure ranges in all seasons. In addition, the RMSEs, as well as their changes with separation distance, also significantly decrease with height (Figures 6a4–6d4).

When the separation distance is less than 10 km, namely, the impact of separation distance on the comparison is expected to be small, the RMSEs are all close to 1 K, except in the lowest pressure range ($p > 850$ hPa) in summer when the mean RMSE values are around 1.5 K (Figure 6b4). The larger RMSEs in summer may be due to the fact that there are more clouds in summer and additional errors occur due to evaporative cooling near the sensor on the aircraft (WMO, 2003). The temperature in the AMDAR data is calculated by the probe temperature and the Mach number, and some measurement error can be introduced by the hypothesis

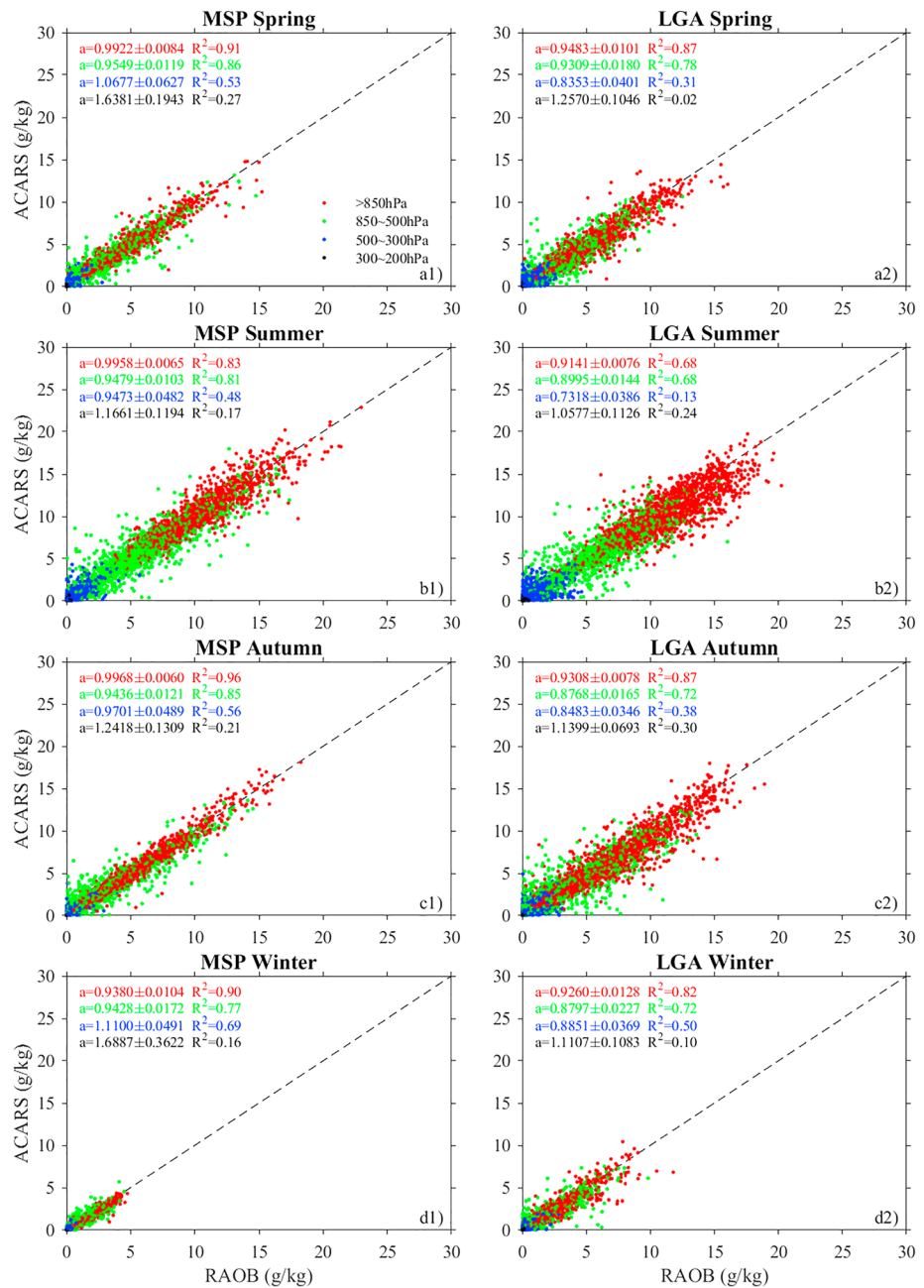


Figure 7. Similar to Figure 5 but for specific humidity and at MSP (left) and LGA (right).

of dry air and the probe recovery factor. Using the fitted linear relations, we can derive the RMSEs of AMDAR data if they were perfectly collocated with radiosondes (i.e., zero separation distance). For the pressure range with $p > 850$ hPa, the RMSEs (MBEs) at zero distance separation are 1.35 (−0.31), 1.52 (−0.32), 1.34 (−0.27), and 1.16 K (−0.16 K) in spring, summer, autumn, and winter, respectively (see also Table 3, which provides a summary). These RMSEs and MBEs suggest that the AMDAR temperature data are reliable given that the uncertainties of AMDAR and radiosonde temperature measurements are about 0.3–0.44 K (WMO, 2003) and more than 0.5 K (Ahnert, 1991; Mapes et al., 2003), respectively.

It is interesting to point out an abnormal site, which is the SAN airport that has a separation distance between AMDAR and the radiosonde station of only 10 km. This airport has an RMSE larger than 3 K. The fitted slope and R^2 value are also much smaller than the other airports with similar separation

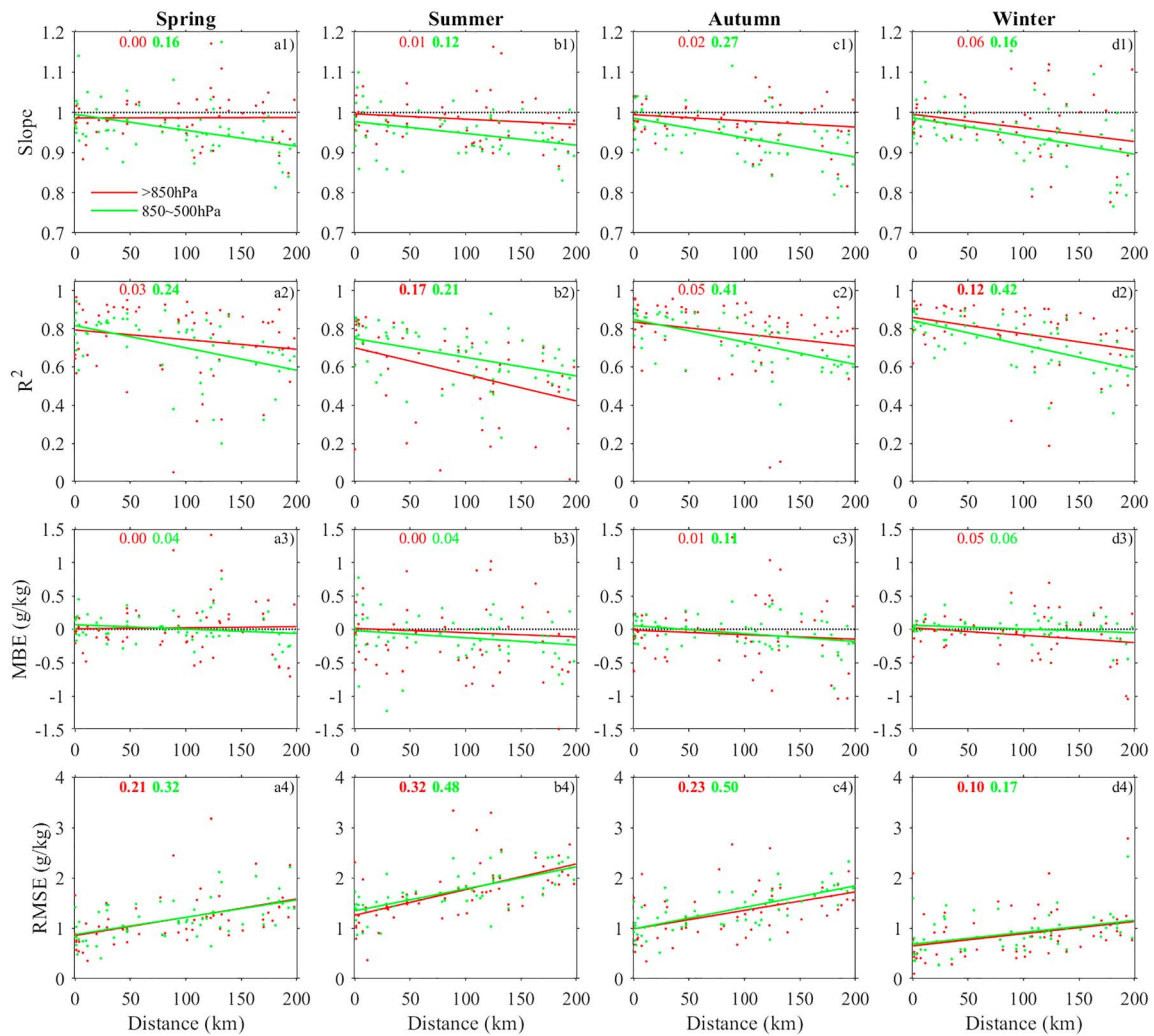


Figure 8. Similar to Figure 6 but for specific humidity and only results at levels with $p > 850$ hPa and 850–500 hPa are shown.

distance. This result is consistent with the individual profile comparisons between AMDAR and radiosonde data near the SAN airport in a recent study by Rahn and Mitchell (2016). This is because most AMDAR observations at the SAN airport are taken while the aircraft flies over the ocean where the temperature remains steady throughout the day. However, the radiosonde data are collected at an inland location where the temperature has a much larger diurnal cycle. If we exclude the SAN airport, the averaged RMSEs (MBEs) within 10 km and for $p > 500$ hPa are 1.20 (−0.11), 1.22 (−0.10), 1.17 (−0.09), and 1.18 K (0.04 K) in spring, summer, autumn, and winter, respectively (see Table 3).

3.2. Humidity

The amount of humidity observations is much less than that of temperature and wind observations as shown in Figure 2. Two different airports MSP and LGA with relatively larger amounts of humidity observations are chosen for our case studies. The distances between the two airports and their nearest corresponding radiosonde stations are 35 and 100 km, respectively. It should be noted that the humidity observations in the AMDAR data are given as dew point temperatures and relative humidity, while in the radiosonde data are given only as dew point temperatures. To compare the actual moisture content in the PBL, the dew point temperature and relative humidity are converted to specific humidity.

The one-to-one scatterplots show that there are dry biases at lower levels ($p > 500$ hPa) at both airports, as indicated by the smaller than unity fitting slopes. In terms of the goodness of fit, the results show good

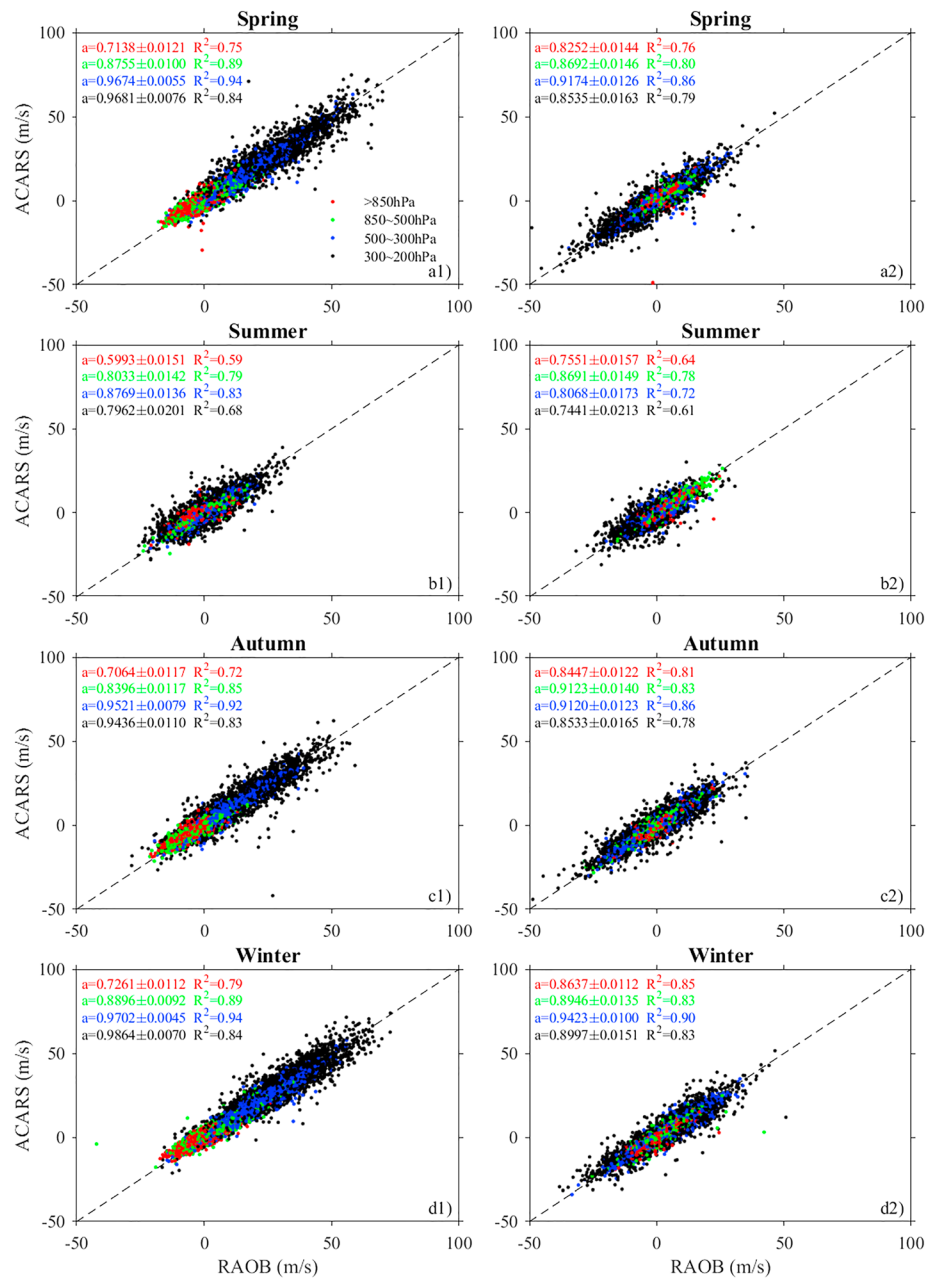


Figure 9. Comparison between AMDAR and RAOB zonal wind (U , left) and meridional wind (V , right) data in different pressure ranges at MIA.

agreement for $p > 500$ hPa but larger bias at the higher levels where the specific humidity is quite small (Figure 7). This is partly because the water vapor contamination within the laser-diode sensing chamber produces moist biases, which prevents the systems from observing very small amounts of atmospheric moisture (Petersen et al., 2006). Although there are errors associated with the humidity observations when the values are small, the WVSS data are still extremely valuable for applications in the region from the ground to about 500 hPa (Petersen et al., 2016). In the lower troposphere (e.g., $p > 850$ hPa), there are larger seasonal variations in the humidity field at MSP than LGA, since the MSP airport is located inland, while the LGA airport is located along the coast. The specific humidity can reach 20 g/kg at both airports in summer but fall to less than 5 g/kg at MSP and 10 g/kg at LGA in winter. Similar to the results of temperatures, the results at LGA are worse possibly due to the larger distance between the airport and the radiosonde station compared to that at MSP.

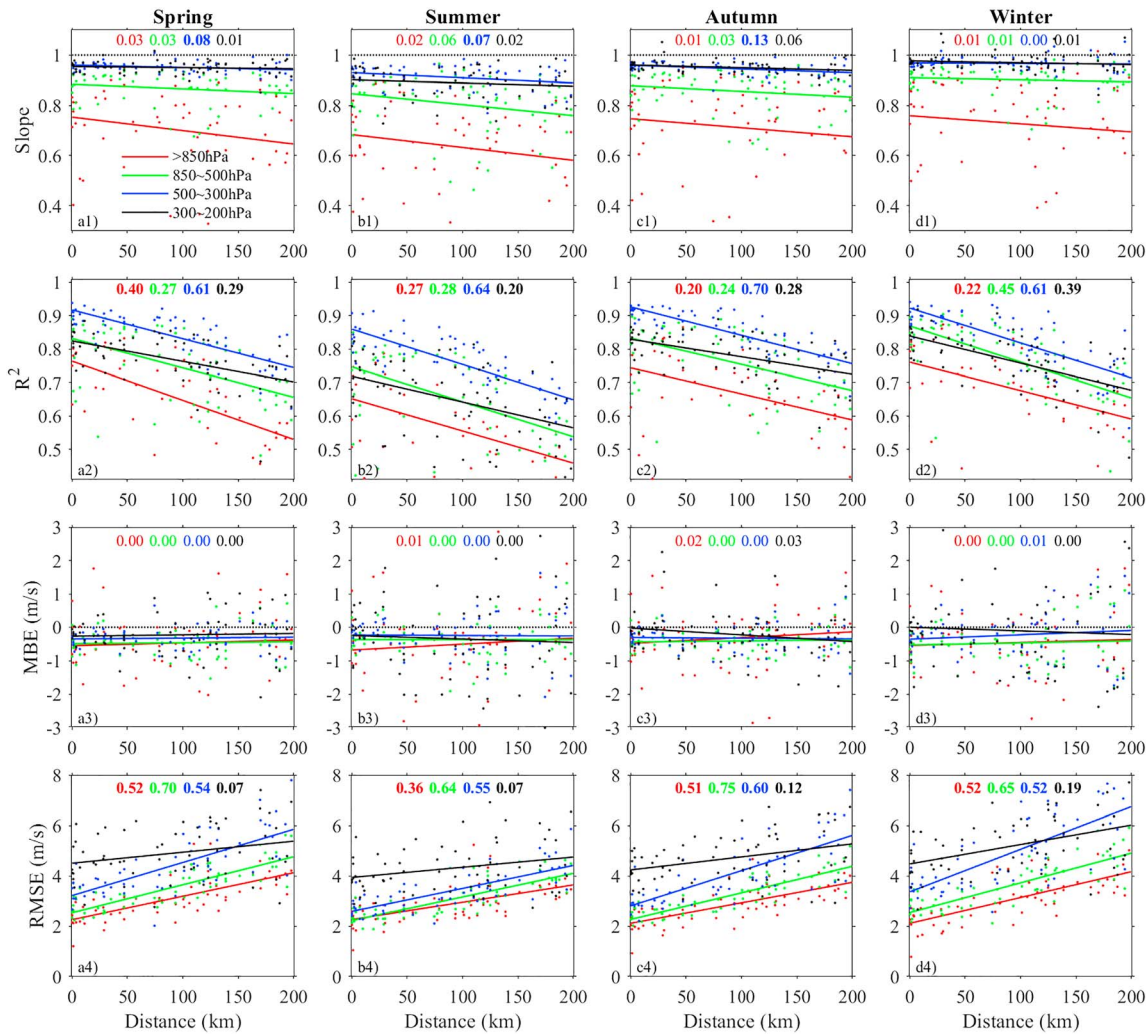


Figure 10. Similar to Figure 6 but for zonal wind (U).

Figure 8 summarizes the results across all 54 airports by again presenting the fitting statistics as a function of the separation distance. Here we only focus on the levels with $p > 500$ hPa because the specific humidity values for $p < 500$ hPa are too small to be well captured by AMDAR as shown in Figure 7. In the following we discuss the results in the two pressure ranges separately. In the lowest pressure range ($p > 850$ hPa), the fitting slopes are close to 1 without any significant trends with the separation distance. Most of the fits are quite good ($R^2 > 0.6$), and the R^2 values decrease with increasing distance as expected. The smaller R^2 values in summer may be related to clouds along the aircraft and/or the radiosonde paths (Petersen et al., 2016). The MBEs show slight dry biases and have no significant trend with the separation distance, which is similar to what the fitting slopes show. The RMSEs are on the order of 1 g/kg with significant increasing trends with the separation distance.

In the pressure range between 850 and 500 hPa, the fitting slopes within 10 km are close to 1 but decrease significantly with increasing separation distance, while the MBEs are small and have no obvious trend. The R^2 and RMSE values decrease and increase with increasing separation distance, respectively. Among the four seasons, it seems that the RMSEs in winter are smaller. This is probably caused by the fact that the specific humidity values are also small in winter.

When the separation distance is less than 10 km, most of the RMSE values are less than 1.5 g/kg in summer and less than 1 g/kg in other seasons, while the MBEs are close to 0, although there is a considerable variability in summer. At perfect collocation (i.e., zero separation distance), the RMSEs (MBEs) inferred from the

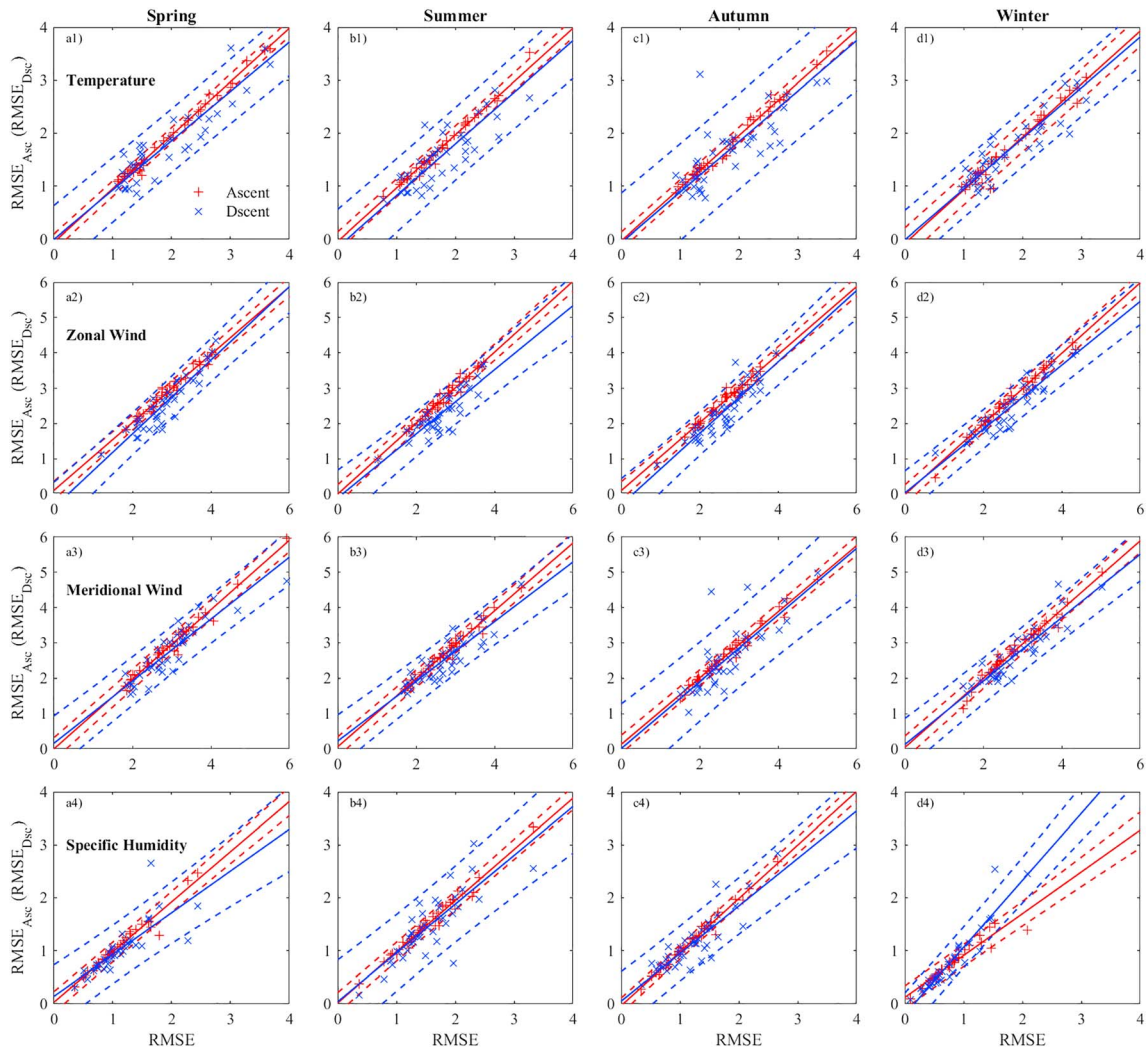


Figure 11. Linear fitting between the total RMSEs of temperature (top panels, unit of K), zonal wind and meridional wind (middle two panels, unit of m/s), and specific humidity (bottom panels, unit of g/kg) and their corresponding ascent (red lines) and descent (blue lines) RMSEs in (a) spring, (b) summer, (c) autumn, and (d) winter in the pressure range with $p > 850$ hPa. The dash lines indicate the 95% confidence intervals.

fitted linear relations are 0.85 (0.01), 1.25 (0.01), 0.98 (−0.01), and 0.64 g/kg (0.02 g/kg) in spring, summer, autumn, and winter, respectively, in the pressure range with $p > 850$ hPa (Table 3). Overall, these results suggest that the AMDAR humidity data agree well with the radiosonde data when they are truly collocated and could be used for a variety of meteorological and climate applications.

3.3. Wind

Wind observations provided by the AMDAR and radiosonde data sets are in terms of wind speed and direction. Since the wind direction cannot be processed in the interpolation, we first convert wind speed and direction to zonal and meridional wind components, hereafter referred as U and V , for comparisons. Figure 9 shows good agreement between AMDAR and radiosonde for both U and V at MIA, where the separation distance is 0 m (Table 2). Compared to temperature, there is a larger degree of variation for wind data, shown by the lower R^2 values. The magnitude of wind components is smaller, and the fits are worse in summer compared to other seasons. It seems that wind speed in the troposphere increases with height, shown as the absolute values of scatter points, with U mainly in the range of -25 – 70 m/s and V mainly in the range of -50 – 50 m/s. The U values in the pressure range 300–200 hPa are mainly positive, which is consistent with the westerlies over CONUS.

Table 4
Annual Mean Numbers of AMDAR Sounding Data Points in the Pressure Ranges of $p > 850$ and $850\text{--}500$ hPa at the Selected Airports, and the Proportion of Ascending Data Points to Total Data Points During the Period 2007–2016

	AIRPORT	>850 hPa	850–500 hPa	Ascending proportion
1	ABQ	/	125,495	0.80
2	BDL	86,390	90,960	0.77
3	BFI	37,409	58,513	0.45
4	BNA	133,086	155,745	0.75
5	BOS	221,653	279,127	0.85
6	BSM	90,304	109,643	0.80
7	BWI	277,771	395,762	0.71
8	CLE	84,486	83,722	0.64
9	DCA	178,625	202,118	0.81
10	DEN	/	479,450	0.75
11	DFW	586,759	949,065	0.90
12	DTW	93,150	125,040	0.65
13	EWR	121,713	165,600	0.76
14	FLL	127,525	168,418	0.80
15	GEG	31,155	47,676	0.79
16	HOU	186,801	251,585	0.71
17	IAD	86,149	106,305	0.77
18	IAH	63,362	66,489	0.77
19	IND	140,426	178,152	0.72
20	JFK	183,934	220,524	0.90
21	LAS	259,641	479,839	0.76
22	LAX	514,644	693,154	0.83
23	LGA	196,897	248,622	0.80
24	MCI	108,298	139,288	0.76
25	MCO	232,449	327,823	0.76
26	MDW	239,335	337,768	0.69
27	MEM	332,626	481,043	0.66
28	MHT	29,955	30,734	0.79
29	MIA	849,228	1,081,936	0.96
30	MSP	113,459	169,936	0.66
31	MSY	84,335	97,756	0.79
32	OAK	203,279	244,411	0.72
33	OKC	35,918	41,562	0.78
34	OMA	35,318	39,236	0.79
35	ONT	123,155	174,603	0.69
36	ORD	341,894	446,132	0.94
37	PDX	191,537	238,752	0.73
38	PHL	203,972	297,395	0.65
39	PHX	251,330	370,054	0.73
40	PIT	48,322	56,051	0.80
41	RDU	88,188	99,042	0.79
42	RNO	9,493	78,701	0.81
43	SAN	209,592	264,978	0.76
44	SAT	76,006	95,027	0.74
45	SDF	241,905	365,163	0.55
46	SEA	528,704	676,339	0.76
47	SFO	188,931	249,865	0.82
48	SJC	146,673	181,398	0.74
49	SLC	14,900	110,651	0.77
50	SMF	113,021	123,390	0.72
51	SNA	149,446	180,306	0.80
52	STL	171,254	203,421	0.78
53	TPA	137,481	175,474	0.78
54	TUL	45,915	47,137	0.88

The comparison across all airports shows negative bias of zonal wind in AMDAR data, indicated by the less than unity fitting slopes and negative MBEs (Figures 10a1–10d1 and 10a3–10d3). This result is consistent with previous studies, which suggest that there are biases toward lower wind speed in the AMDAR data than radiosondes (e.g., Rahn & Mitchell, 2016; Schwartz & Benjamin, 1995). The goodness of fitting in the pressure range with $p > 850$ hPa shows large variations, although the R^2 values remain over 0.6 in summer and over 0.7 in other seasons when the separation distances are small. The fits at the upper levels are much better, especially in the range 500–300 hPa where the R^2 values within 10 km are around 0.8 in summer and around 0.9 in other seasons (Figures 10a2–10d2). The RMSEs increase with height (Figures 10a4–10d4), suggesting that the RMSEs are associated with the wind speed magnitude, which also increases with height (Gao et al., 2012). This is also consistent with previous studies (e.g., Ding et al., 2015). The RMSEs show significantly increasing trends with the separation distance. Seasonal variations of the RMSEs mainly exist at the upper two levels, where RMSEs are smaller in summer. The results for meridional wind are very similar to those for zonal wind and thus are not shown. At zero separation distance, the RMSEs (MBEs) of zonal wind for $p > 850$ hPa are 2.25 (–0.55), 2.26 (–0.68), 2.11 (–0.48), and 2.11 m/s (–0.54 m/s), while the fitted RMSEs (MBEs) of meridional wind for $p > 850$ hPa are 2.26 (–0.17), 2.18 (–0.29), 2.00 (–0.01), and 2.15 m/s (0.13 m/s) in spring, summer, autumn, and winter, respectively (Table 3).

Compared to temperature and humidity, the wind RMSEs are relatively large. The large RMSEs in the wind observations are mainly caused by the uncertainties of both AMDAR and radiosonde observational systems. The uncertainty of wind speed in the AMDAR reports is 2–3 m/s (WMO, 2003). In addition, the wind data in AMDAR are calculated from the difference vector between the ground speed and the air speed and the air speed is determined by the Mach number and the probe temperature in the Pitot system. Thus, in addition to the inherent system error, temperature errors also lead to wind errors (Moninger et al., 2003). The radiosonde wind speed uncertainty is also 2–3 m/s provided by previous studies (Hoehne, 1980; Mapes et al., 2003). Considering these uncertainties, it can be concluded that the wind observations in the AMDAR reports are reasonably accurate enough for PBL investigations.

3.4. Dependence on Flight Phases

In the AMDAR dataset, the flight phase is identified as cruise, ascent, or descent. Since the cruise phase was excluded in the data set that we used, comparison is conducted only between ascents and descents. Note that in the raw data there is also an unsteady phase but it is not a separate phase and can be encountered during any other phases. To do so, the profiles generated by using only ascents or descents are compared to radiosonde data. We find that the fitting slopes and the goodness between ascent and descent profiles are very close (not shown). We only compare the ascent and descent RMSEs to the RMSEs without separating ascents and descents (hereafter the total RMSEs).

Figure 11 shows the results for temperature, wind, and humidity for $p > 850$ hPa. The ascent RMSE values are slightly larger than the descent RMSE values, in general, except for winter specific humidity. The ascent

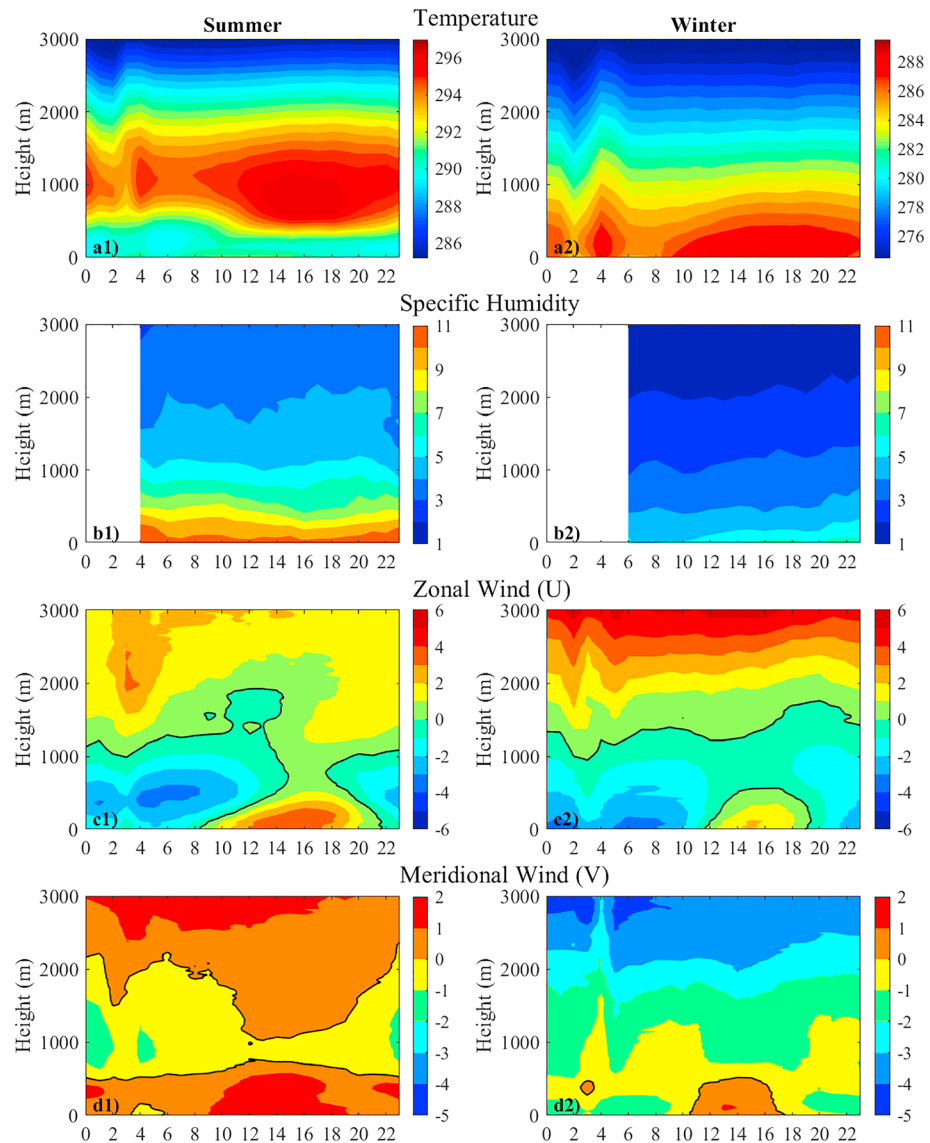


Figure 12. Diurnal variations of (a) temperature (K), (b) specific humidity (g/kg), (c) zonal wind (U , m/s), and (d) meridional wind (V , m/s) in the lowest 3,000 m above the ground averaged over summer (left) and winter (right) from 2007 to 2016 at LAX. The solid black lines indicate zero values.

RMSE values show little difference from the total RMSEs, while the descent RMSE values are slightly smaller than the total RMSE values and have much larger uncertainties. This is because ascent reports generally dominate the AMDAR data set (Ballish & Kumar, 2006; Petersen et al., 2016) and the uncertainty generally decreases as the number of measurements increases (Drosg, 2009; Drüe et al., 2010). In the data set we used, the fractions of ascent soundings averaged over all airports are 0.84 and 0.71 for the pressure ranges with $p > 850$ and 850–500 hPa, respectively (Table 4). However, the 95% confidence intervals of ascent and descent RMSEs overlap well, indicating that there are no significant differences in the biases between ascent and descent data. The only exception is winter humidity (Figure 11d4), where the fitting lines are strongly affected by several abnormally large RMSE values. Even so, the confidence intervals of the ascent and descent RMSE values when they are less than 2 g/kg still overlap well.

The differences in the ascent and descent data in the pressure range 850–500 hPa are even smaller than those in the pressure range with $p > 850$ hPa for temperature, wind, and humidity and have smaller uncertainty (not shown). Overall, these results suggest that compared to the biases (estimated from collocated

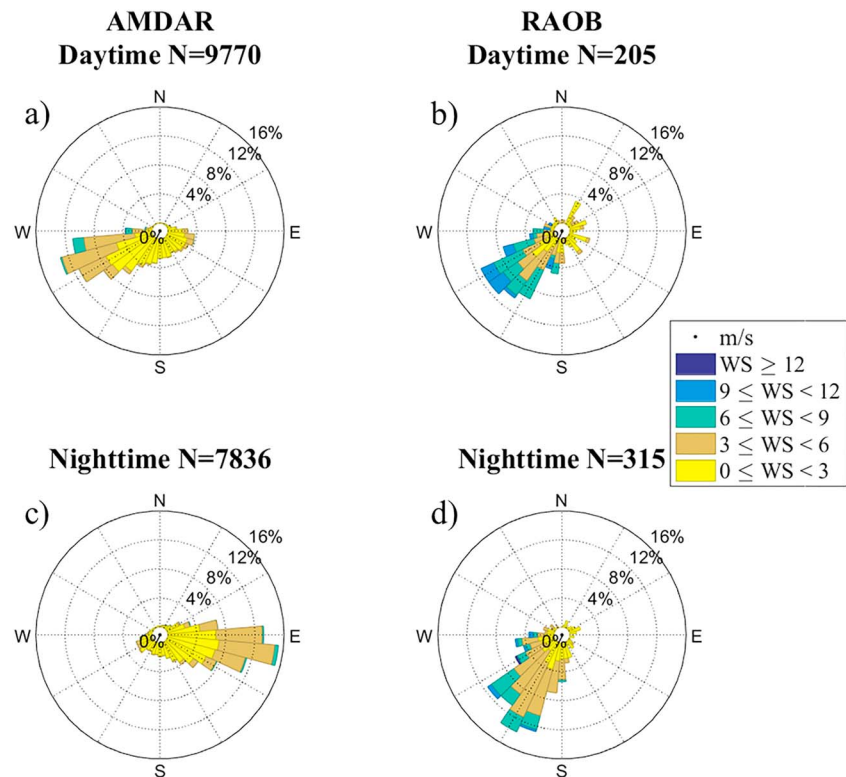


Figure 13. The wind roses from AMDAR (left) and RAOB (right) data averaged over 0–500 m during daytime (up) and nighttime (bottom) in summer at LAX. N indicates the number of samples.

radiosonde data), the dependence on flight phases will hardly affect the accuracy of the produced hourly AMDAR profiles.

3.5. Applications of the New Data Record

In this section, we demonstrate the unique value of the new data record of PBL profiles in studying the diurnal variation of the PBL, including the land-sea breeze effects. Compared to the radiosonde data, the AMDAR data have much higher temporal resolutions and can adequately resolve the diurnal variation of the PBL. Figure 12 presents the 10-year averaged summer and winter diurnal variations of temperature, humidity, and winds at LAX. The blank areas are hours in which the total number of profiles within the 10-year period (2007–2016) is less than 20 for temperature and winds and 10 for specific humidity. Note that local standard time is used. At LAX, which is located along the western coast, there are significant differences in the PBL temperature between summer and winter (Figures 12a1 and 12a2). Temporally, the maximum temperature occurs around 16:00 in summer while around 12:00 in winter. Vertically, the maximum temperature happens at around 1,000 m while near the surface in winter. This vertical distribution of temperature in summer is driven in part by the land-sea breeze effects. As shown in Figures 12c1–12d1, during daytime (08:00–19:00), sea breeze ($U > 0$) at the lower layer transports cold air from the sea to the land, while warmer air rises over land due to the surface heating and blows from the land to the sea at the upper layer ($U < 0$). The opposite occurs during nighttime. Thus, the temperature over the LAX airport in summer is affected by cold advection at the lower level and warm advection at the upper level in both daytime and nighttime, which leads to the vertical distribution of temperature. In winter, the effect of land-sea breeze is much weaker than that in summer (Figures 12c2–12d2). Compared to the zonal wind (U), which is more indicative of the land-sea breeze, the meridional wind (V) shows a smaller magnitude and a smaller diurnal variation in the PBL (Figures 12d1 and 12d2).

To further demonstrate the advantage of AMDAR data in capturing the land-sea breeze effects, Figure 13 present the summer wind rose from AMDAR and RAOB data, which have been averaged from the

surface to 500 m above the surface, during daytime and nighttime. Here daytime is defined as 08:00–19:00 local time, while the remaining hours represent nighttime. The AMDAR wind speeds and directions are broadly consistent with the climatological results in Figure 12. There is an evident inverse in the wind direction between day and night, especially when the wind speed is larger than 3 m/s (Figures 13a and 13c), indicating a typical land-sea breeze phenomenon. Note that there are always southerly winds during daytime and nighttime, which corresponds to the all-day positive meridional wind near the surface shown in Figure 12d1. Compared to the AMDAR data, the radiosonde data simply cannot capture the land-sea breeze but show southwestern winds during both daytime and nighttime (Figures 13b and 13d). This is largely because (1) the radiosonde data are typically only available twice a day and (2) the radiosonde station is located inland while the LAX airport is located at the coast. In this study, there are two radiosonde stations located within 200 km from the LAX airport (Table 2). The inland one is chosen for the comparison in Figure 13 because the other one provides much fewer observations.

In summary, the AMDAR data can capture the land-sea breeze effects much better than the traditional radiosonde data, including the transition between sea breeze and land breeze (see Figure 12) that is impossible with the twice-daily radiosonde data. Overall, the high temporal resolution feature of the AMDAR data makes them better suited for studying the diurnal variation of the PBL.

4. Conclusions

AMDAR reports provide a large amount of temperature, wind, and humidity observations with high temporal resolutions. In this study, the AMDAR data collected near 54 airports over CONUS from 2007 to 2016 are analyzed. Based on the aircraft data taken from ascents and descents, a data record of hourly PBL profiles is developed by merging all soundings within 1 hr and interpolating to a regular vertical grid. This new data set of PBL and lower troposphere profiles at temporal resolutions not affordable by conventional observing systems will offer a great opportunity to investigate the diurnal variation of PBL.

Comparisons between AMDAR and radiosonde data are conducted at 43 airports, which have nearby radiosonde stations. The maximum separation between the two data sources is limited to 200 km in space (and 1 hr in time implicitly). Overall, the comparison results show that AMDAR data agree quite well with the radiosonde data. The AMDAR temperature data show warm biases at high altitudes ($p < 500$ hPa), but such warm biases become insignificant at low altitudes ($p > 850$ hPa). The finding of warm biases at high altitudes is consistent with previous studies that focused on the AMDAR data during the cruise phase (Ballish & Kumar, 2008). The insignificant biases at low altitudes make the AMDAR data more suitable for studying PBL processes. Consistent with a recent review study (Petersen et al., 2016), the AMDAR specific humidity data are of good quality when compared to the radiosonde measurements, with slight dry biases in the pressure range with $p > 500$ hPa. The AMDAR wind data show consistently negative biases at all levels.

The RMSEs between AMDAR and radiosonde data generally decrease with height for temperature and specific humidity, while increase with height for wind. The RMSEs of humidity and wind are positively correlated with their magnitude, which explains why the humidity RMSEs at lower levels are larger and why the wind RMSEs are smaller in summer than in other seasons. Compared to RMSEs, the MBEs for temperature, humidity, and wind are much smaller.

The RMSEs between AMDAR and radiosonde data are highly dependent on the separation distance, especially at lower levels ($p > 850$ hPa) where the atmosphere is less homogeneous, while the dependence of MBE on the separation distance is much weaker except for temperature in the pressure range with $p > 850$ hPa. In particular, in the pressure range with $p > 850$ hPa (e.g., within the PBL), the AMDAR data become consistently warmer than the radiosonde data as the separation distance increases. The RMSEs and MBEs when the two data sets are truly collocated (i.e., zero distance separations) are quantified. Specifically, the RMSEs of temperature for $p > 850$ hPa are approximately 1.3 K, and the MBEs fall between -0.16 K and -0.32 K. The RMSEs of specific humidity for $p > 850$ hPa are 1.25 g/kg in summer and less than 1 g/kg in other seasons, while the MBEs of specific humidity for $p > 850$ hPa are close to 0. For wind components, the RMSEs are relatively large. The RMSEs for $p > 850$ hPa are approximately 2.2 m/s for both zonal and meridional wind, but the absolute values of MBEs are less than 0.7 m/s.

It is further found that the dependence of RMSEs on flight phases (ascent or descent) at levels with $p > 500$ hPa can be ignored in the AMDAR data applications. This is because the RMSEs of ascent and descent data are close and the fraction of ascent soundings in the AMDAR data set exceeds 70% at most airports. Hence, it does not add any value, at least from the perspective of generating a data record of diurnal PBL profiles, to separate ascents and descents.

In summary, the overall quality of AMDAR data is close to that of radiosonde data. Although the AMDAR reports typically have a few hours from the midnight to early morning that have no data and the produced data record is only available near airports, this data record will be of great value for studying the diurnal PBL structures and land-sea/lake breeze effects, as demonstrated in our paper, and a variety of other applications such as land-atmosphere coupling investigations and air pollution modeling. Lastly, it is important to acknowledge that the evaluation of the AMDAR data quality is conducted at the resolution of the radiosonde data, which is coarser than the resolution of the AMDAR data. Future work assessing the AMDAR data quality with higher-resolution reference data, especially in the PBL, is still needed.

Acknowledgments

We thank Professor David Rahn at University of Kansas for kindly sharing the code computing height from pressure altitude and Dr. Weilin Liao at Sun Yat-sen University for helping produce Figure 1. Y. J. Z. and Z. Q. G. are supported by the National Natural Science Foundation of China under grant 41705004 and the Natural Science Foundation of Jiangsu Province under grant SBK2017041444. Y. J. Z. is also supported by the Talent Start-up Foundation of Nanjing University of Information Science and Technology under grant 2016r056 and the scholarship under the State Scholarship Fund (201708320030). D. L. acknowledges support from the Initiative on Cities at Boston University and US Army Research Office (grant W911NF-18-1-0360). The AMDAR and radiosonde data are downloaded from the Meteorological Assimilation Data Ingest System (MADIS) web service portal (<https://madis-data.cprk.ncep.noaa.gov/madisPublic1/data/archive/>), and the ISD data are downloaded from National Oceanic and Atmospheric Administration (NOAA) at <https://www.ncdc.noaa.gov/isd/data-access>. The processed profiles can be obtained from the corresponding author upon request.

References

- Ahnert, P. (1991). Precision and comparability of National Weather Service upper air measurements. In *Symposium on Meteorological Observations and Instrumentations, 7th* (pp. 221–226). New Orleans, LA.
- Ballish, B. A., & Kumar, V. K. (2006). Comparison of aircraft and radiosonde temperature biases at NCEP. In Proceedings of 10th Symposium on Integrated Observing and Assimilation Systems for the Atmosphere, Oceans and Land Surface (IOAS-AOLS), Boston, USA.
- Ballish, B. A., & Kumar, V. K. (2008). Systematic differences in aircraft and radiosonde temperatures: Implications for NWP and climate studies. *Bulletin of the American Meteorological Society*, 89(11), 1689–1708. <https://doi.org/10.1175/2008BAMS2332.1>
- Benjamin, S. G., Schwartz, B. E., & Cole, R. E. (1999). Accuracy of ACARS wind and temperature observations determined by collocation. *Weather and Forecasting*, 14(6), 1032–1038. [https://doi.org/10.1175/1520-0434\(1999\)014<1032:AOAWAT>2.0.CO;2](https://doi.org/10.1175/1520-0434(1999)014<1032:AOAWAT>2.0.CO;2)
- Cardinali, C., Isaksen, L., & Andersson, E. (2003). Use and impact of automated aircraft data in a global 4DVAR data assimilation system. *Monthly Weather Review*, 131(8), 1865–1877. <https://doi.org/10.1175/2569.1>
- Corner, B. R., Palmer, R. D., & Larsen, M. F. (1999). A new radiosonde system for profiling the lower troposphere. *Journal of Atmospheric and Oceanic Technology*, 16(7), 828–836. [https://doi.org/10.1175/1520-0426\(1999\)016<0828:ANRSFP>2.0.CO;2](https://doi.org/10.1175/1520-0426(1999)016<0828:ANRSFP>2.0.CO;2)
- Ding, J., Zhuge, X.-Y., Wang, Y., & Xiong, A. (2015). Evaluation of Chinese Aircraft Meteorological Data Relay (AMDAR) weather reports. *Journal of Atmospheric and Oceanic Technology*, 32(5), 982–992. <https://doi.org/10.1175/JTECH-D-14-00145.1>
- Drosg, M. (2009). *Dealing with uncertainties: A guide to error analysis*. Berlin, Heidelberg: Springer Science & Business Media. <https://doi.org/10.1007/978-3-642-01384-3>
- Drüe, C., Frey, W., Hoff, A., & Hauf, T. (2008). Aircraft type-specific errors in AMDAR weather reports from commercial aircraft. *Quarterly Journal of the Royal Meteorological Society*, 134(630), 229–239. <https://doi.org/10.1002/qj.205>
- Drüe, C., Hauf, T., & Hoff, A. (2010). Comparison of boundary-layer profiles and layer detection by AMDAR and WTR/RASS at Frankfurt airport. *Boundary-Layer Meteorology*, 135(3), 407–432. <https://doi.org/10.1007/s10546-010-9485-0>
- Ek, M., & Mahrt, L. (1994). Daytime evolution of relative humidity at the boundary layer top. *Monthly Weather Review*, 122(12), 2709–2721. [https://doi.org/10.1175/1520-0493\(1994\)122<2709:DEORHA>2.0.CO;2](https://doi.org/10.1175/1520-0493(1994)122<2709:DEORHA>2.0.CO;2)
- Ek, M. B., & Holtslag, A. A. M. (2004). Influence of soil moisture on boundary layer cloud development. *Journal of Hydrometeorology*, 5(1), 86–99. [https://doi.org/10.1175/1525-7541\(2004\)005<0086:IOSMOB>2.0.CO;2](https://doi.org/10.1175/1525-7541(2004)005<0086:IOSMOB>2.0.CO;2)
- Gao, F., Zhang, X., Jacobs, N. A., Huang, X.-Y., Zhang, X., & Childs, P. P. (2012). Estimation of TAMDAR observational error and assimilation experiments. *Weather and Forecasting*, 27(4), 856–877. <https://doi.org/10.1175/WAF-D-11-00120.1>
- Garratt, J. R. (1994). The atmospheric boundary layer. *Earth-Science Reviews*, 37(1–2), 89–134. [https://doi.org/10.1016/0012-8252\(94\)90026-4](https://doi.org/10.1016/0012-8252(94)90026-4)
- Hoehne, W. E. (1980). Precision of National Weather Service upper air measurements, NOAA, Tech. Memo. NWST&ED-16. National Oceanic and Atmospheric Administration/National Weather Service (23 pp.).
- Ingleby, B., Pauley, P., Kats, A., Ator, J., Keyser, D., Doerenbecher, A., et al. (2016). Progress toward high-resolution, real-time radiosonde reports. *Bulletin of the American Meteorological Society*, 97(11), 2149–2161. <https://doi.org/10.1175/BAMS-D-15-00169.1>
- Isaksen, L., Vasiljevic, D., Dee, D., & Healy, S. (2012). Bias correction of aircraft data implemented in November 2011. *ECMWF Newsletter*, 131(6).
- Lindvall, J., & Svensson, G. (2015). The diurnal temperature range in the CMIP5 models. *Climate Dynamics*, 44(1–2), 405–421. <https://doi.org/10.1007/s00382-014-2144-2>
- Lindvall, J., Svensson, G., & Hannay, C. (2013). Evaluation of near-surface parameters in the two versions of the atmospheric model in CESM1 using flux station observations. *Journal of Climate*, 26(1), 26–44. <https://doi.org/10.1175/JCLI-D-12-00020.1>
- Lott, N. (2004). The quality control of the integrated surface hourly database, Preprints, 14th Conf. on Applied Climatology. Seattle, WA, Amer. Meteor. Soc., 7.8.
- Mapes, B. E., Ciesielski, P. E., & Johnson, R. H. (2003). Sampling errors in rawinsonde-array budgets. *Journal of the Atmospheric Sciences*, 60(21), 2697–2714. [https://doi.org/10.1175/1520-0469\(2003\)060<2697:SEIRB>2.0.CO;2](https://doi.org/10.1175/1520-0469(2003)060<2697:SEIRB>2.0.CO;2)
- Miloshevich, L. M., Vömel, H., Paukkunen, A., Heymsfield, A. J., & Oltmans, S. J. (2001). Characterization and correction of relative humidity measurements from Vaisala RS80—A radiosondes at cold temperatures. *Journal of Atmospheric and Oceanic Technology*, 18(2), 135–156. [https://doi.org/10.1175/1520-0426\(2001\)018<0135:CACORH>2.0.CO;2](https://doi.org/10.1175/1520-0426(2001)018<0135:CACORH>2.0.CO;2)
- Moninger, W. R., Benjamin, S. G., Jamison, B. D., Schlatter, T. W., Smith, T. L., & Szoke, E. J. (2010). Evaluation of regional aircraft observations using TAMDAR. *Weather and Forecasting*, 25(2), 627–645. <https://doi.org/10.1175/2009WAF2222321.1>
- Moninger, W. R., Mamros, R. D., & Pauley, P. M. (2003). Automated meteorological reports from commercial aircraft. *Bulletin of the American Meteorological Society*, 84(2), 203–216. <https://doi.org/10.1175/BAMS-84-2-203>

- Oke, T. R. (1982). The energetic basis of the urban heat island. *Quarterly Journal of the Royal Meteorological Society*, 108(455), 1–24.
- Petersen, R. A. (2016). On the impact and benefits of AMDAR observations in operational forecasting—Part I: A review of the impact of automated aircraft wind and temperature reports. *Bulletin of the American Meteorological Society*, 97(4), 585–602. <https://doi.org/10.1175/BAMS-D-14-00055.1>
- Petersen, R. A., Crouce, L., Mamrosh, R., Baker, R., & Pauley, P. (2016). On the impact and future benefits of AMDAR observations in operational forecasting—Part II: Water vapor observations. *Bulletin of the American Meteorological Society*, 97(11), 2117–2133. <https://doi.org/10.1175/BAMS-D-14-00211.1>
- Petersen, R. A., Feltz, W., Olson, E., & Bedka, S. (2006). Evaluation of the WVSS-II moisture sensor using co-located in-situ and remotely sensed observations. In *10th Symposium on Integrated Observing and Assimilation Systems for the Atmosphere, Oceans, and Land Surface*.
- Rahn, D. A., & Mitchell, C. J. (2016). Diurnal climatology of the boundary layer in southern California using AMDAR temperature and wind profiles. *Journal of Applied Meteorology and Climatology*, 55(5), 1123–1137. <https://doi.org/10.1175/JAMC-D-15-0234.1>
- Santanello, J. A., Dirmeyer, P. A., Ferguson, C. R., Findell, K. L., Tawfik, A. B., Berg, A., Ek, M., et al. (2018). Land–atmosphere interactions: The LoCo perspective. *Bulletin of the American Meteorological Society*, 99(6), 1253–1272. <https://doi.org/10.1175/BAMS-D-17-0001.1>
- Schwartz, B., & Benjamin, S. G. (1995). A comparison of temperature and wind measurements from ACARS-equipped aircraft and rawinsondes. *Weather and Forecasting*, 10(3), 528–544. [https://doi.org/10.1175/1520-0434\(1995\)010<0528:ACOTAW>2.0.CO;2](https://doi.org/10.1175/1520-0434(1995)010<0528:ACOTAW>2.0.CO;2)
- Stull, R. B. (2012). *An introduction to boundary layer meteorology* (Vol. 13). Dordrecht, Netherlands: Springer Science & Business Media.
- Walther, G.-R., Post, E., Convey, P., Menzel, A., Parmesan, C., Beebee, T. J. C., Fromentin, J. M., et al. (2002). Ecological responses to recent climate change. *Nature*, 416(6879), 389–395. <https://doi.org/10.1038/416389a>
- World Meteorological Organization (2003). *Aircraft Meteorological Data Relay (AMDAR) reference manual*, WMO Publ. WMO-958 (p. 80). Geneva, Switzerland: Secretariat of the World Meteorological Organization.
- Wulfmeyer, V., Hardesty, R. M., Turner, D. D., Behrendt, A., Cadeddu, M. P., Di Girolamo, P., Schlüssel, P., et al. (2015). A review of the remote sensing of lower tropospheric thermodynamic profiles and its indispensable role for the understanding and the simulation of water and energy cycles. *Reviews of Geophysics*, 53, 819–895. <https://doi.org/10.1002/2014RG000476>
- Zhu, Y., Derber, J. C., Purser, R. J., Ballish, B. A., & Whiting, J. (2015). Variational correction of aircraft temperature bias in the NCEP's GSI analysis system. *Monthly Weather Review*, 143(9), 3774–3803. <https://doi.org/10.1175/MWR-D-14-00235.1>